Published for SISSA by Springer

Received: *September 21, 2023*
Accepted: *January 2, 2024*
Published: *January 19, 2024*

Measurement of the τ lepton polarization in Z boson decays in proton-proton collisions at $\sqrt{s} = 13$ TeV

The CMS collaboration

E-mail: cms-publication-committee-chair@cern.ch

Abstract: The polarization of τ leptons is measured using leptonic and hadronic τ lepton decays in $\mathrm{Z} \to \tau^+\tau^-$ events in proton-proton collisions at $\sqrt{s} = 13$ TeV recorded by CMS at the CERN LHC with an integrated luminosity of $36.3\,\mathrm{fb}^{-1}$. The measured τ^- lepton polarization at the Z boson mass pole is $\mathcal{P}_\tau(\mathrm{Z}) = -0.144 \pm 0.006\,(\mathrm{stat}) \pm 0.014\,(\mathrm{syst}) = -0.144 \pm 0.015$, in good agreement with the measurement of the τ lepton asymmetry parameter of $A_\tau = 0.1439 \pm 0.0043 = -\mathcal{P}_\tau(\mathrm{Z})$ at LEP. The τ lepton polarization depends on the ratio of the vector to axial-vector couplings of the τ leptons in the neutral current expression, and thus on the effective weak mixing angle $\sin^2\theta_{\mathrm{W}}^{\mathrm{eff}}$, independently of the Z boson production mechanism. The obtained value $\sin^2\theta_{\mathrm{W}}^{\mathrm{eff}} = 0.2319 \pm 0.0008(\mathrm{stat}) \pm 0.0018(\mathrm{syst}) = 0.2319 \pm 0.0019$ is in good agreement with measurements at e^+e^- colliders.

Keywords: Hadron-Hadron Scattering, Tau Physics

ArXiv ePrint: 2309.12408

https://doi.org/10.1007/JHEP01(2024)101

Contents

1 Introduction

Measuring standard model (SM) parameters with high precision in various processes may reveal yet unknown physics phenomena as deviations from SM predictions. One of the fundamental parameters is the effective weak mixing angle $\sin^2\theta_W^{\text{eff}}$, which leads to different couplings for right- and left-handed fermions in weak neutral currents. A consequence of this difference is the effective polarization of fermion-antifermion pairs in Z boson decays. The τ^- lepton polarization is defined as $\mathcal{P}_\tau = (\sigma_+ - \sigma_-)/(\sigma_+ + \sigma_-)$, where σ_+ and σ_- are the cross sections for the production of τ^- leptons with positive and negative helicities, respectively.

The helicity of τ leptons from Z boson decays can be measured from energy and angular distributions of the τ lepton decay products. The polarization measures the ratio of vector to axial-vector neutral current couplings of the τ lepton, and therefore this ratio provides

JHEP01(2024)101

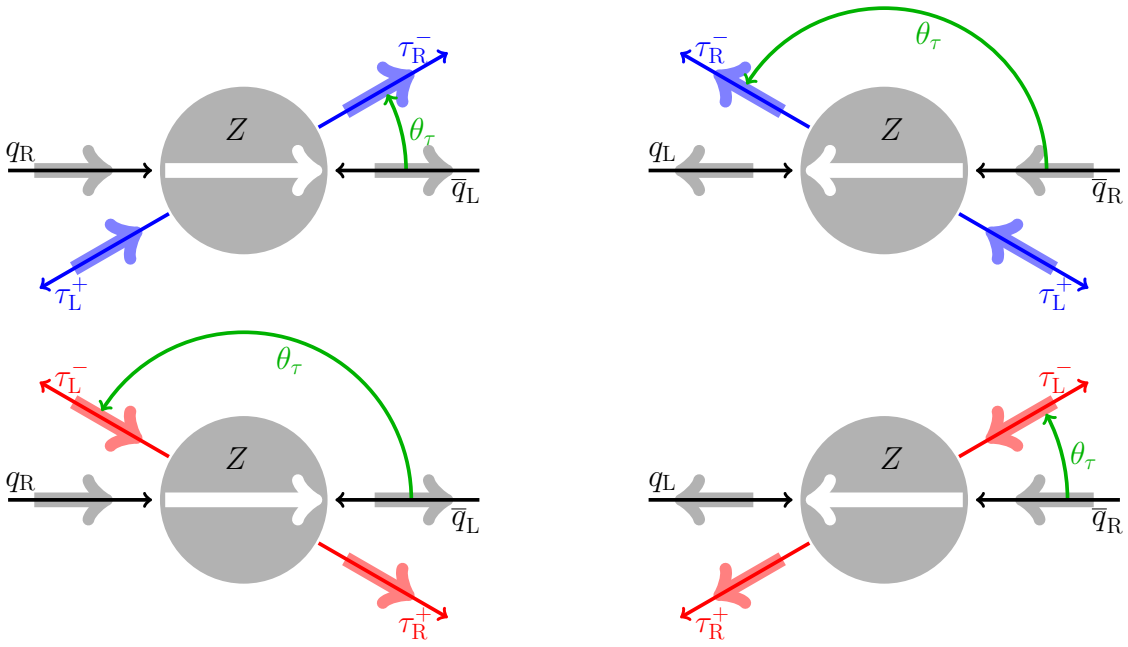

Figure 1. The four possible helicity states of incoming quarks and outgoing τ leptons. Thin arrows depict the direction of movement and the thick arrows show the spin of the particles. The angle θ_τ is the scattering angle of the τ^- lepton with respect to the quark momentum in the rest frame of the Z boson.

a further measurement of the weak mixing angle solely from τ lepton couplings as detailed in the following.

In $Z \to \tau^+\tau^-$ events, the helicity of the τ^+ lepton is expected to have a sign opposite to that of the τ^- helicity. The differential cross section for the process $q\bar{q} \to Z \to \tau^+\tau^-$ can be expressed at the lowest order [1]:

$$\frac{d\sigma}{d\cos\theta_\tau} = F_0(\hat{s})(1+\cos^2\theta_\tau) + 2F_1(\hat{s})\cos\theta_\tau - \lambda_\tau[F_2(\hat{s})(1+\cos^2\theta_\tau) + 2F_3(\hat{s})\cos\theta_\tau]. \quad (1.1)$$

Here θ_τ is the scattering angle of the τ^- with respect to the quark momentum in the rest frame of the Z boson, as illustrated in figure 1. The symbol λ_τ denotes the sign of positive or negative helicity of the τ^- lepton and $\hat{s}$ is the squared center-of-mass energy of the $q\bar{q}$ pair. The $F_i(\hat{s})$ are structure functions for the initial and final fermion pairs describing the strength and shape of the Z resonance and its dependence on the vector and axial-vector neutral-current coupling constants. The total cross section is:

$$\sigma = \sum_{\lambda_\tau=\pm1} \int \frac{d\sigma}{d\cos\theta_\tau} d\cos\theta_\tau. \quad (1.2)$$

From the cross section in eq. (1.1), the following quantities can be determined: the asymmetry A_{FB} of the forward-backward cross sections, the polarization $\mathcal{P}_\tau$ of the τ^- lepton, and the

JHEP01(2024)101

forward-backward polarization asymmetry $A_{\mathrm{FB}}^{\mathrm{pol}}$:

$$\begin{aligned} A_{\mathrm{FB}} &= \frac{1}{\sigma}[\sigma(\cos\theta_\tau > 0) - \sigma(\cos\theta_\tau < 0)] = \frac{3F_1(\hat{s})}{4F_0(\hat{s})}, \\ \mathcal{P}_\tau &= \frac{1}{\sigma}[\sigma(\lambda_\tau = +1) - \sigma(\lambda_\tau = -1)] = -\frac{F_2(\hat{s})}{F_0(\hat{s})}, \\ A_{\mathrm{FB}}^{\mathrm{pol}} &= \frac{1}{\sigma}[\mathcal{P}_\tau(\cos\theta_\tau > 0) - \mathcal{P}_\tau(\cos\theta_\tau < 0)] = -\frac{3F_3(\hat{s})}{4F_0(\hat{s})}, \end{aligned} \tag{1.3}$$

where the symbols F_i correspond to the structure functions in eq. (1.1).

The cross section includes the contributions from Z boson exchange, photon exchange, and photon-Z interference. If $\sqrt{\hat{s}}$ is equal to the Z boson mass M_{Z}, the contributions from photon exchange cancel in the numerator of the asymmetries and the following holds:

$$\begin{aligned} A_{\mathrm{FB}} &= \frac{3}{4}A_{\mathrm{f}}A_\tau, \\ \mathcal{P}_\tau &= -A_\tau, \\ A_{\mathrm{FB}}^{\mathrm{pol}} &= \frac{3}{4}A_{\mathrm{f}}, \end{aligned} \tag{1.4}$$

where $A_\tau = 2v_\tau a_\tau/(v_\tau^2 + a_\tau^2)$ and $A_{\mathrm{f}} = 2v_{\mathrm{f}}a_{\mathrm{f}}/(v_{\mathrm{f}}^2 + a_{\mathrm{f}}^2)$ are the asymmetry parameters defined by the effective neutral current vector and axial-vector couplings v_τ and a_τ for the τ lepton, and v_{f} and a_{f}, the parameters for the initial-state fermions, respectively. In the limit $v_\tau \ll a_\tau$, the polarization can be written as $\mathcal{P}_\tau \approx -2v_\tau/a_\tau$, and is simply related to $\sin^2\theta_{\mathrm{W}}^{\mathrm{eff}}$:

$$\mathcal{P}_\tau = -A_\tau = -\frac{2v_\tau a_\tau}{v_\tau^2 + a_\tau^2} \approx -2\frac{v_\tau}{a_\tau} = -2(1 - 4\sin^2\theta_{\mathrm{W}}^{\mathrm{eff}}). \tag{1.5}$$

Hence, a measurement of the polarization $\mathcal{P}_\tau$ can provide a precise determination of $\sin^2\theta_{\mathrm{W}}^{\mathrm{eff}}$ using only τ lepton couplings. Comparison with the value of $\sin^2\theta_{\mathrm{W}}^{\mathrm{eff}}$ measured in the process $\mathrm{e^+e^-} \to \mathrm{Z}$ at LEP [2–5] tests the lepton universality of the weak neutral current.

Since τ leptons decay rapidly inside the detector, their polarization is measured by analyzing the energy and direction of their decay products. Observables used for this analysis are the angles and momenta of the daughter particles with respect to the boost direction of the τ lepton or intermediate particles in the decay of the τ lepton.

Measurements of the τ lepton polarization have been performed in $\mathrm{e^+e^-}$ annihilation by the four LEP experiments at center-of-mass energies near M_{Z} [2–5], at the linear collider experiment SLD [6], and in proton-proton (pp) collisions by the ATLAS experiment at the CERN LHC at $\sqrt{s} = 8\,\mathrm{TeV}$ [7].

The measurement of the τ lepton polarization in Z boson decays was pioneered at LEP [1], where the polarization could be measured in a very small window around the Z pole and as a function of the polar emission angle $\cos\theta_\tau$ of the τ lepton with respect to the incoming electrons. A maximum likelihood fit to this angular dependence provides the best measurement of the polarization.

A complication occurs when the polarization is measured in pp collisions; in contrast to $\mathrm{e^+e^-}$ collisions, the polar emission angle θ_τ is not, or only very poorly, known and can not be

JHEP01(2024)101

used in the analysis. Furthermore, instead of a fixed value, measurements are always an average over a limited range of the center-of-mass energy of the $\mathrm{d\bar{d}}$ and $\mathrm{u\bar{u}}$ quark-antiquark pairs. The measurement is effectively an integration over the experimental width of the Z boson and a fairly wide range of its rapidity and transverse momentum p_{T}. The ranges are determined by the parton distribution functions (PDFs) of the proton and the acceptance of the experiment.

In this paper, a measurement of the τ^- lepton polarization $\mathcal{P}_\tau$ is presented, based on $\mathrm{Z} \to \tau\tau$ events in pp collisions with parton-parton center-of-mass energies $\sqrt{\hat{s}}$ of 75–120 GeV. The measurement is performed by using the following combinations of leptonic and hadronic decay modes of the τ leptons: $\tau_\mathrm{e}\tau_\mu$, $\tau_\mathrm{e}\tau_\mathrm{h}$, $\tau_\mu\tau_\mathrm{h}$, and $\tau_\mathrm{h}\tau_\mathrm{h}$, where the symbol τ_e refers to the decay $\tau^- \to \mathrm{e}^-\bar{\nu}_\mathrm{e}\nu_\tau$, the symbol τ_μ refers to the decay $\tau^- \to \mu^-\bar{\nu}_\mu\nu_\tau$, and the τ_h to the hadronic τ decay modes.

Following a short description of the CMS experiment in section 2 and of the Data and Monte Carlo samples (section 3), the event reconstruction and the event selection are detailed in sections 4 and 5, respectively. The background estimates are described in section 6, before the τ lepton spin variables are discussed in section 7. After a discussion of systematic uncertainties in section 8, the measurement of the τ^- lepton polarization $\mathcal{P}_\tau$ is described in section 9. Finally, from the measurement of $\mathcal{P}_\tau$, averaged over the mass range of the Z boson, the effective weak mixing angle $\sin^2\theta_\mathrm{W}^\mathrm{eff}$ is derived and presented in section 10. The paper ends with a summary in section 11.

2 The CMS detector

The central feature of the CMS apparatus is a superconducting solenoid of 6 m internal diameter, providing a magnetic field of 3.8 T. Within the magnetic volume are a silicon pixel and strip tracker, a lead tungstate crystal electromagnetic calorimeter (ECAL), and a brass and scintillator hadron calorimeter (HCAL), each composed of a barrel and two endcap sections. Forward calorimeters extend the pseudorapidity (η) coverage provided by the barrel and endcap detectors. Muons are detected in gas-ionization chambers embedded in the steel flux-return yoke outside the solenoid. A more detailed description of the CMS detector, together with a definition of the coordinate system used and the relevant kinematical variables, are reported in ref. [8].

Events of interest are selected using a two-tiered trigger system. The first level (L1), composed of custom hardware processors, uses information from the calorimeters and muon detectors to select events at a rate of around 100 kHz within a fixed latency of 4 μs [9]. The second level, known as the high-level trigger (HLT), consists of a farm of processors running a version of the full event reconstruction software optimized for fast processing, and reduces the event rate to around 1 kHz before data storage [10].

3 Data and Monte Carlo samples

This analysis is based on pp collision data at a center-of-mass energy of 13 TeV collected in the year 2016 with the CMS detector at the LHC. The analyzed data correspond to an integrated luminosity of 36.3 fb^{-1} [11].

JHEP01(2024)101

A Drell-Yan (DY) signal Monte Carlo (MC) sample of $Z/\gamma^* \to \tau\tau$ events is generated for this analysis at next-to-leading order (NLO) in quantum chromodynamics (QCD), but at leading order (LO) for electromagnetic processes using MadGraph5_aMC@NLO v2.4.2 [12], with the hadronization step simulated by pythia 8 [13]. The CUETP8M1 [14] pythia tune and pythia 8 v8.226 are used. The τ polarization flag TauDecays:externalMode = 0 is used to ensure proper τ decay simulation by tauola 1.1.6 [15, 16] following the helicity assignment of MadGraph5_aMC@NLO. The NNPDF3.0 [17] PDFs are used. A sample of about 60 million events was produced in this way and processed through the detector simulation and reconstruction chain. The simulation of the detector response is based on Geant4 [18].

Differences in the mass and p_T distributions of the τ pair between data and simulations are observed and 2D weights based on these variables are derived and applied to simulated Drell-Yan events [19]. Since MadGraph5_aMC@NLO is NLO in QCD, additional jets are included at the matrix element level. A reweighting between 3.9 and 12.3% was applied to the distribution of the number of generated partons in the event to match the distribution of jets. The analysis is not sensitive to those additional jets.

The main background processes, such as W+jets and other Drell-Yan processes like $Z/\gamma^* \to ee$ and $Z/\gamma^* \to \mu\mu$, are generated at LO for electromagnetic processes with MadGraph5_aMC@NLO and interfaced with pythia 8 with the tune CUETP8M1 [14]. Backgrounds from s-channel and tW single top quark associated production are generated with powheg v1.0 [20] and powheg v2.0 [21], respectively, interfaced to pythia 8 with the CUETP8M1 tune. The top quark pair production ($t\bar{t}$) sample is produced with powheg v1.0 [22] interfaced to pythia 8 with the CUETP8M2T4 [23] tune. Diboson samples are generated with MadGraph5_aMC@NLO and tune CUETP8M1, interfaced to pythia 8 and τ lepton decays are processed by tauola. Again, the NNPDF3.0 [17] PDFs are used for the background processes.

The impact of multiple pp collisions in the same or adjacent bunch crossings (pileup) on event reconstruction [24] is accounted for in simulation by superimposing simulated minimum bias pp events on top of each process of interest. Because the distribution of the number of pileup events in the simulation is not the same as in data, the simulation is weighted to match the data.

4 Event reconstruction

The particle-flow (PF) algorithm [25] reconstructs and identifies each individual particle in an event, with an optimized combination of information from the various elements of the CMS detector. The energy of photons is obtained from the ECAL measurement. The energy of electrons is determined from a combination of the electron momentum at the primary vertex (PV) as determined by the tracker, the energy of a corresponding ECAL cluster, and the energy sum of all bremsstrahlung photons spatially compatible with originating from the electron track. The energy of muons is obtained from the curvature of the corresponding track. The energy of charged hadrons is determined from a combination of their momentum measured in the tracker and the matching ECAL and HCAL energy deposits, corrected for

JHEP01(2024)101

the response function of the calorimeters to hadronic showers. Finally, the energy of neutral hadrons is obtained correspondingly from the corrected ECAL and HCAL energies.

The PV is taken to be the vertex corresponding to the hardest scattering in the event, evaluated from the largest value of summed physics-object p_{T}^2 as described in ref. [19].

For each event, hadronic jets are clustered from these reconstructed particles based on the infrared- and collinear-safe anti-k_{T} algorithm [26, 27] with a distance parameter of 0.4. The jet momentum is determined as the vector sum of all particle momenta in the jet, and is found from simulation to be, on average, within 5-10% of the generated momentum over the entire p_{T} spectrum and detector acceptance. Pileup interactions can lead to additional tracks and calorimetric energy depositions to the jet momentum. To mitigate this effect, charged particles identified to be originating from pileup vertices are discarded, and an offset correction is applied to correct for remaining contributions. Jet energy corrections are derived from simulation to bring the measured response of jets to that of particle level jets on average. In situ measurements of the momentum balance in dijet, photon+jet, Z+jet, and multijet events are used to account for any residual differences in the jet energy scale between data and simulation. The jet energy resolution amounts typically to 15–20% at 30 GeV, 10% at 100 GeV, and 5% at 1 TeV [28]. Additional selection criteria are applied to each jet to remove jets potentially dominated by anomalous contributions from various subdetector components or reconstruction failures.

Electrons are reconstructed within the geometric acceptance $|\eta| < 2.5$. The momentum resolution for electrons with $p_{\mathrm{T}} \approx 45$ GeV from $\mathrm{Z} \to \mathrm{e}^{+}\mathrm{e}^{-}$ decays ranges from 1.6 to 5.0%. It is generally better in the barrel region than in the endcaps, and also depends on the bremsstrahlung energy emitted by the electron before reaching the ECAL [29].

Muons are measured in the range $|\eta| < 2.4$, with detection planes made out of three types of gas-ionization detectors: drift tubes, cathode strip chambers, and resistive-plate chambers. Matching muons to tracks measured in the silicon tracker results in a relative transverse momentum resolution of 1% in the barrel and 3% in the endcaps for muons with p_{T} up to 100 GeV [30].

The missing transverse momentum vector $\vec{p}_{\mathrm{T}}^{\,\mathrm{miss}}$ in the event is defined as the negative vector sum of the momenta of all reconstructed particles in an event projected onto the plane perpendicular to the beam axis. It is computed from the PF candidates weighted by their probability to originate from the PV [31]. Recoil corrections are applied to account for mismodeling of $\vec{p}_{\mathrm{T}}^{\,\mathrm{miss}}$ in the simulated samples of Drell-Yan and W+jets production. The vector $\vec{p}_{\mathrm{T}}^{\,\mathrm{miss}}$ is further modified to account for corrections to the energy scale of the reconstructed jets in the event. The pileup-per-particle identification algorithm [32] is applied to reduce the pileup dependence of the $\vec{p}_{\mathrm{T}}^{\,\mathrm{miss}}$ observable. The magnitude of $\vec{p}_{\mathrm{T}}^{\,\mathrm{miss}}$ is referred to as $p_{\mathrm{T}}^{\mathrm{miss}}$.

Leptonic τ decays, τ_{e} and τ_{μ}, are identified as isolated electrons and muons. The lepton ℓ (e, μ) isolation $I_{\mathrm{rel}}(\ell)$ is defined by the following equation:

$$I_{\mathrm{rel}}(\ell) = \frac{\sum_{\text{ch. had}} p_{\mathrm{T}} + \max\left(0,\ \sum_{\text{n. had.}} E_{\mathrm{T}} + \sum_{\gamma} E_{\mathrm{T}} - \beta(\mathrm{PU})\right)}{p_{\mathrm{T}}^{\ell}}. \tag{4.1}$$

In this expression, $\sum_{\text{ch. had}} p_{\mathrm{T}}$ is the scalar transverse momentum sum of the charged hadrons originating from the PV within a cone of size $\Delta R = \sqrt{(\Delta\eta)^2 + (\Delta\phi)^2} = 0.3$ or 0.4 for electrons

JHEP01(2024)101

and muons, respectively, centered on the lepton. The quantities $\Delta\eta$ and $\Delta\phi$ measure the particle separation in η and of the azimutal angle ϕ in radians. The sum $\sum_{\text{n. had.}} E_{\text{T}} + \sum_{\gamma} E_{\text{T}}$ in eq. (4.1) represents a similar quantity for neutral particles.

To estimate the contribution of neutral particles due to pileup the so-called effective-area method is used for identified electrons. The pileup in this method is estimated as $\beta(\text{PU}) = \rho A_{\text{eff}}$, where ρ is the event-specific average pileup energy density per unit area in the $\eta - \phi$ plane and A_{eff} is the effective area specific to the given type of isolation.

A different method is used for the selected muons; the contribution of photons and neutral hadrons originating from pileup vertices $\beta(\text{PU})$ is estimated from the scalar transverse momentum sum of charged hadrons originating from pileup vertices: $\beta(\text{PU}) = 0.5 \sum_{\text{PU}} p_{\text{T}}$. The sum $\sum_{\text{PU}} p_{\text{T}}$ is multiplied by a factor of 0.5, which corresponds approximately to the ratio of neutral-to-charged hadron production, as estimated from simulation.

Lepton isolation and identification efficiencies are measured with a tag-and-probe method [33, 34] using $\text{Z} \to \ell^+\ell^-$ events in lepton p_{T} and η bins from samples collected based on single-lepton triggers.

The reconstruction of the hadronically decaying τ leptons (τ_{h} candidates) is performed by the hadron-plus-strips algorithm (HPS) [34]. Jets are reconstructed from PF constituents with the anti-k_{T} algorithm [26] with a distance parameter of $\Delta R = 0.4$. They are considered as τ_{h} candidates if they comprise one or three charged hadrons with a net charge of ± 1, and up to two neutral pions. Dedicated attention is given to photons originating from $\pi^0 \to \gamma\gamma$ decays likely to convert to e^+e^- pairs, by collecting the photon and electron constituents, called strips, in an area around the jet direction in the $\eta - \phi$ plane. The size of the strip varies as a function of the p_{T} of the τ_{h}. To further characterize the τ_{h} signature, its visible reconstructed mass is required to be compatible with that of the $\rho(770)$ resonance for $\tau^- \to \text{h}^-\pi^0$ signatures, and the $\text{a}_1(1260)$ resonance for $\tau^- \to \text{h}^-\pi^0\pi^0$ and $\tau^- \to \text{h}^-\text{h}^-\text{h}^+$ signatures, with corresponding channels for the τ^+.

Energy scale corrections are computed for each decay mode using either the visible mass of both τ leptons or the invariant mass distributions of the $\pi^\pm\pi^0$, $\pi^\pm\pi^0\pi^0$, and $\pi^+\pi^-\pi^\pm$ systems. The correction factors are chosen such that either the visible mass distributions of both τ leptons of the MC events match the data distribution, or the invariant mass distributions of the $\pi^\pm\pi^0$, $\pi^\pm\pi^0\pi^0$, and $\pi^+\pi^-\pi^\pm$ systems match the shapes of the ρ and a_1 resonances [34].

In this analysis, since the decay channels of the τ_{h} have different polarization sensitivity, it is fundamental to identify these channels correctly. To increase the purity of the reconstructed decay channels, a multi-class multivariate analysis (MVA) with a boosted decision tree algorithm (implemented using the XGBoost library) is applied in addition to the HPS algorithm. The multivariate algorithm was developed for the analysis of the charge-conjugation and parity (CP) properties of the Higgs boson in $\tau^+\tau^-$ decays [35], which is also very sensitive to migrations between reconstructed decay modes. Based on the simulated DY signal sample, the use of the multivariate algorithm in addition to the HPS algorithm increased the purity of the $\tau^- \to \pi^-\nu$ and $\tau^- \to \rho^-\nu$ channels in the analysis presented here from 63 to 83% and from 63 to 77%, respectively. For reconstructed τ leptons the efficiencies for the correct decay mode identifications are 76, 82 and 94% for the decays $\tau^- \to \pi^-\nu$, $\tau^- \to \rho^-\nu$ and $\tau^- \to \pi^-\pi^+\pi^-\nu$, respectively.

JHEP01(2024)101

Channel	Trigger	Lepton selection	Additional selection	
$\tau_e\tau_\mu$	$p_T^\mu > 8\,\text{GeV}, p_T^e > 23\,\text{GeV}$ or $p_T^\mu > 23\,\text{GeV}, p_T^e > 12\,\text{GeV}$	$p_T^e > 15\,\text{GeV}, \lvert\eta^e\rvert < 2.4$ $p_T^\mu > 15\,\text{GeV}, \lvert\eta^\mu\rvert < 2.4$ $p_T^\ell > 24\,\text{GeV}$ for lead trigger leg	$I_{\text{rel}}(e) < 0.15$ $I_{\text{rel}}(\mu) < 0.20$	
$\tau_e\tau_h$	$p_T^e > 25\,\text{GeV}$	$p_T^e > 30\,\text{GeV}, \lvert\eta^e\rvert < 2.1$ $p_T^{\tau_h} > 30\,\text{GeV}, \lvert\eta^{\tau_h}\rvert < 2.3$	$I_{\text{rel}}(e) < 0.15$ Med DeepTau WP	$m_T^e < 50\,\text{GeV}$
$\tau_\mu\tau_h$	$p_T^\mu > 22\,\text{GeV}$ or $p_T^\mu > 19\,\text{GeV}, p_T^{\tau_h} > 20\,\text{GeV}$	$p_T^\mu > 23\,\text{GeV}, \lvert\eta^\mu\rvert < 2.1$, $p_T^\mu > 20\,\text{GeV}$ $p_T^{\tau_h} > 30\,\text{GeV}, \lvert\eta^{\tau_h}\rvert < 2.3$	$I_{\text{rel}}(\mu) < 0.15$ Med DeepTau WP	$m_T^\mu < 50\,\text{GeV}$
$\tau_h\tau_h$	$p_T^{\tau_h} > 35\,\text{GeV}, p_T^{\tau_h} > 35\,\text{GeV}$	$p_T^{\tau_h} > 45(40)\,\text{GeV}, \lvert\eta^{\tau_h}\rvert < 2.1$	Med DeepTau WP	

Table 1. Selections applied in this analysis. For the $\tau_\mu\tau_h$ channel two triggers were used with different muon thresholds, the p_T selection threshold for τ_h refers to both. For the $\tau_h\tau_h$ channel, the p_T selection threshold for the nonleading τ_h was lower by 5 GeV. The label Med DeepTau WP in the last column refers to the medium working point of the DeepTau discriminator against fake τ_h.

The DeepTau discriminator [36] is used in this analysis in order to distinguish τ_h from quark and gluon jets, electrons and muons. It is a deep neural network algorithm that returns three discriminants, trained to reduce misreconstruction of jets, electrons, or muons as τ_h candidates. The so-called Medium Working Point (Med DeepTau WP) is used for τ_h as referred to in table 1 of the next section.

Correction factors were measured in ref. [34] for the different working points of anti-jet, anti-electron, and anti-muon discriminators used to identify the τ_h. These were measured in $Z \to \tau_\mu\tau_h$ events, considering the visible mass of the muon or τ lepton candidate as observables (or alternatively the number of tracks in the signal and isolation cones).

5 Event selection and categorization

The following analysis uses selection criteria developed for the analyses of the Higgs boson in the $\tau^+\tau^-$ decay channel [19] and its CP properties [35]; some of them are summarized in table 1.

A combination of several triggers is used to cover the different channels of the $Z \to \tau^+\tau^-$ decays and described in more detail in ref. [19]. The off-line selection thresholds in table 1 are often significantly higher than the trigger threshold to ensure exactly known efficiencies. The pseudorapidity limits come from trigger and object reconstruction constraints.

The electrons and muons in the $\tau_e\tau_\mu$ channel, electron, muon and τ_h in the $\tau_e\tau_h$, $\tau_\mu\tau_h$ channel, respectively, and the two τ_h in the $\tau_h\tau_h$ channel are required to be oppositely charged. The τ_e, τ_μ and τ_h candidates are required to have a distance of closest approach to the PV of $|d_z| < 0.2\,\text{cm}$ in the direction along the beam axis and $|d_{xy}| < 0.045\,\text{cm}$ in the transverse plane.

In the $\tau_e\tau_h$ channel, the trigger system requires at least one isolated electron object, whereas in the $\tau_e\tau_\mu$ channel, the triggers rely on the presence of both an electron and a

JHEP01(2024)101

muon, allowing lower online p_T thresholds. In the $\tau_\mu\tau_h$ channel, events are selected with at least one isolated muon trigger candidate, or at least one isolated muon and one τ_h trigger candidate, depending on the offline muon p_T.

For the $\tau_h\tau_h$ channel, the trigger selects events with two τ_h objects using a less restrictive isolation criteria [34] than the more selective Med DeepTau WP used for the analysis listed in table 1.

The $\tau\tau$ final states are categorized according to the number of identified electrons and muons in the event. Events containing an electron and a muon are assigned to the $\tau_e\tau_\mu$ category. If at least one τ_e and τ_h candidate is found, but no muon, the event is assigned the $\tau_e\tau_h$ final state. Similarly the event is assigned to the $\tau_\mu\tau_h$ final state if it contains at least one muon candidate, but no electron. If neither an electron nor a muon is found but at least two τ_h candidates, the event is assigned to the $\tau_h\tau_h$ final state. Events containing three or more electrons or muons are vetoed to suppress the contribution from other Drell-Yan events. This ensures that the four final states are mutually exclusive and of very good purity.

The τ_e, τ_μ, and τ_h candidates corresponding to the decay of the τ lepton pair are required to be separated by $\Delta R > 0.3$ for $\tau_e\tau_\mu$ events and $\Delta R > 0.5$ for $\tau_e\tau_h$, $\tau_\mu\tau_h$, $\tau_h\tau_h$ events. Since τ_h candidates are wider than τ_ℓ the required separation is slightly larger. The reconstructed leptons must correspond to the HLT candidates on which the trigger decision is made. The correspondence is ensured by requiring the selected electron or muon in the $\tau_e\tau_h$ and $\tau_\mu\tau_h$ final states to be within a distance $\Delta R = 0.5$ from the corresponding HLT objects. The same spatial separation is applied for both τ_h candidates in the $\tau_h\tau_h$ final state.

The transverse mass m_T^ℓ is defined from the transverse momentum p_T^ℓ of the electron or muon and the missing transverse momentum:

$$m_T^\ell = \sqrt{2p_T^\ell p_T^{\text{miss}}(1 - \cos[\Delta\phi(\ell, \vec{p}_T^{\text{miss}})])}. \tag{5.1}$$

Events containing a W boson are expected to have large values of m_T due to the missing neutrino, hence a selection on m_T less than 50 GeV is applied to reduce this background.

After the event selection described above, events are categorized according to the reconstructed decay mode of the hadronically decaying τ leptons.

6 Background estimation

The largest background comes from multijet events where one of the jets is misidentified as a τ_h. Based on simulation it represents about 84% of the expected background in the $\tau_h\tau_h$ channel, and 16 (20%) in the $\tau_e\tau_h$ ($\tau_\mu\tau_h$) channels. Drell-Yan events in dilepton final states may contribute if either a lepton is identified as a τ_h or an additional jet is misidentified as τ_h. These contributions are suppressed by rejecting events containing lepton pairs with same flavor and opposite electric charge and applying the DeepTau discriminants to suppress electrons and muons wrongly reconstructed as τ_h candidates. Whereas control samples are used in data to evaluate the multijet background, other contributions such as $t\bar{t}$ and electroweak processes (EWK: single top quark, Z +jets, and dibosons) rely on simulation. The W+jets background is significant in the $\tau_\mu\tau_h$ and $\tau_e\tau_h$ final states (respectively about 31 and 27% of the expected background) and is evaluated from data as described below.

JHEP01(2024)101

6.1 The $\tau_e\tau_h$ and $\tau_\mu\tau_h$ final states

The QCD multijet and W+jets background estimates are obtained by applying the so-called *ABCD* method to four regions, delimited by the lepton (e or μ) isolation and the lepton-τ_h pair charge combinations, opposite-sign (OS) or same-sign (SS) pairs. The signal region A is defined by $I_{\text{rel}}(\ell) < 0.15$ and an OS pair; B by $I_{\text{rel}}(\ell) < 0.15$ and an SS pair; C by $I_{\text{rel}}(\ell) > 0.15$ and an OS pair; D by $I_{\text{rel}}(\ell) > 0.15$ and an SS pair. These regions receive significant contributions from W+jets events that must be evaluated simultaneously with the multijet background. Therefore, two samples are defined in which the *ABCD* method is used: one (low-m_{T}) follows the signal selection criteria for which the transverse mass satisfies $m_{\text{T}} < 50\,\text{GeV}$; and the other (high-$m_{\text{T}}$) is enriched in W+jets events by requiring $m_{\text{T}} > 70\,\text{GeV}$. The high-$m_{\text{T}}$ region enriched by W+jets is used to evaluate the W+jets background in the $I_{\text{rel}}(\ell) < 0.15$ isolation regions from the ratio between high-m_{T} and low-m_{T}.

The number of multijet background events (QCD) in the signal region is given by:

$$N^{\text{QCD}}_{\text{low-}m_{\text{T}}}(A) = N^{\text{QCD}}_{\text{low-}m_{\text{T}}}(B)\ f^{\text{OS/SS}}_{\text{low-}m_{\text{T}}}. \tag{6.1}$$

Here $f^{\text{OS/SS}}_{\text{low-}m_{\text{T}}}$ is the ratio of the number of events for data in the C and D regions where non-QCD events were subtracted. $N^{\text{QCD}}_{\text{low-}m_{\text{T}}}(B)$ is the number of events $N_{\text{low-}m_{\text{T}}}(B)$ observed in region B, where EWK and W+jets backgrounds were subtracted:

$$N^{\text{QCD}}_{\text{low-}m_{\text{T}}}(B) = N_{\text{low-}m_{\text{T}}}(B) - N^{\text{EWK}}_{\text{low-}m_{\text{T}}}(B) - N^{\text{W}}_{\text{low-}m_{\text{T}}}(B). \tag{6.2}$$

$N^{\text{W}}_{\text{low-}m_{\text{T}}}(B)$ is obtained from the high-m_{T} region:

$$N^{\text{W}}_{\text{low-}m_{\text{T}}}(B) = N^{\text{W}}_{\text{high-}m_{\text{T}}}(B)\ f^{\text{SS}}_{\text{low-}m_{\text{T}}/\text{high-}m_{\text{T}}}. \tag{6.3}$$

The high-m_{T} region is enriched in W+jets events, EWK background estimates obtained from simulation are nevertheless subtracted. The ratio $f^{\text{SS}}_{\text{low-}m_{\text{T}}/\text{high-}m_{\text{T}}}$ is obtained from simulated W+jets events.

Similarly, the W+jets yield in the signal region A is given by:

$$N^{\text{W}}_{\text{low-}m_{\text{T}}}(A) = N^{\text{W}}_{\text{high-}m_{\text{T}}}(A)\ f^{OS}_{\text{low-}m_{\text{T}}/\text{high-}m_{\text{T}}}. \tag{6.4}$$

To limit statistical fluctuations relaxed criteria on the muon and τ_h isolations ($I_{\text{rel}}(\ell) < 0.3$ and medium isolation for τ_h) are used to obtain $f^{OS}_{\text{low-}m_{\text{T}}/\text{high-}m_{\text{T}}}$.

6.2 The $\tau_h\tau_h$ final state

The multijet background estimation differs for the $\tau_h\tau_h$ final state since the W+jets background is negligible for this final state. A sideband region is defined from which the yields and shapes are obtained. This sideband region is the same as the signal region except that the isolation requirements of the two τ_h candidates are relaxed, $I_{\text{rel}}(\ell) < 0.15$ for a tight and $I_{\text{rel}}(\ell) > 0.15$ for a loose selection. The purpose of relaxing the criteria for both τ leptons, and not only for one, is to gain in statistical precision. The extrapolation from the sideband region to the signal region to estimate the QCD contribution N_{QCD} is obtained by applying a so called loose-to-tight isolation scale factor, denoted $f^{\text{SS}}_{\text{tight/loose}}$:

$$N^{\text{QCD}} = f^{\text{SS}}_{\text{tight/loose}} N^{\text{OS}}_{\text{loose}}. \tag{6.5}$$

JHEP01(2024)101

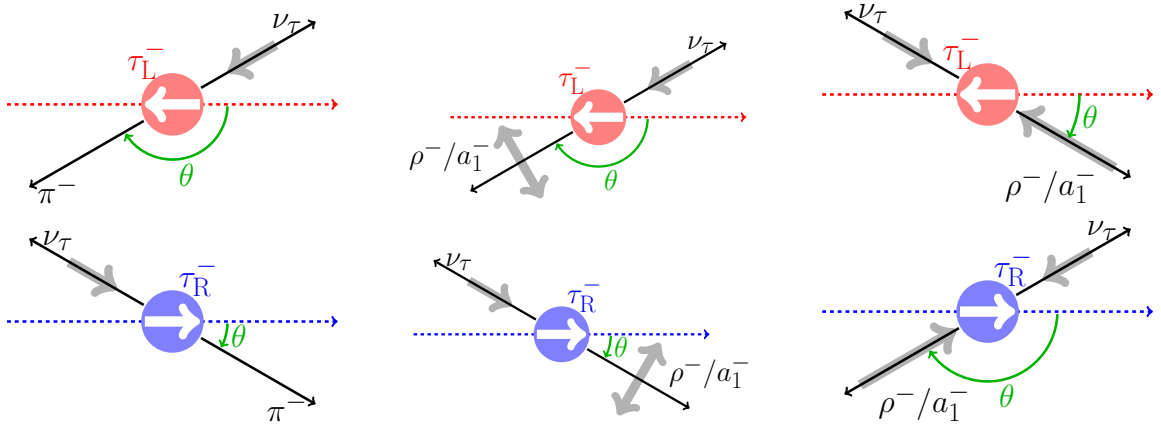

Figure 2. Definition of the angle θ in the τ^- lepton rest frame for the decays $\tau^- \to h^-\nu$ ($h^- = \pi^-, \rho^-, a_1^-$), upper row for left-handed τ lepton τ_L^-, lower row for right-handed τ lepton τ_R^-. The thick arrows indicate the spin directions of the particles.

This scale factor is computed in SS events, $f^{SS}_{tight/loose} = N^{SS}_{tight}/N^{SS}_{loose}$. The number of events measured in the three regions, namely N^{OS}_{loose}, N^{SS}_{tight}, and N^{SS}_{loose} is evaluated by removing the residual EWK backgrounds estimated by a MC simulation.

7 Tau lepton spin observables

7.1 Decay angles

The spin of the τ lepton is transferred into the total angular momentum of its decay products. Therefore, the orientation of the spin of the τ lepton can be revealed from the angular distributions of the decay products relative to the direction of the τ lepton momentum and relative to each other.

Figure 2 illustrates the relation between the τ^- lepton helicity and the polarization of the decay products. The first angle to consider is the angle θ between the boost direction of the τ lepton projected onto the τ lepton rest frame and the momentum direction of the hadron.

$$\cos\theta = \vec{n}_\tau \cdot \vec{n}_{h^\pm} = 2\frac{E(h^\pm)}{E(\tau^\pm)} - 1, \tag{7.1}$$

where $\vec{n}_\tau$ and $\vec{n}_{h^\pm}$ are unit vectors in the τ lepton rest frame pointing in the τ boost direction and along the hadron momentum, respectively. The quantities $E(h^\pm)$ and $E(\tau^{\pm})$ are the energies of the hadron and τ lepton in the laboratory frame, respectively. In the case of a leptonic τ^- lepton decay, the vector of the hadron is replaced by the one of the lepton, but two neutrinos are emitted instead of one, leading to a more complicated situation. In the experimentally favored case where the charged lepton takes most of the τ^- lepton energy, the neutrino and anti-neutrino are emitted collinear and the pair is opposite to the charged lepton, and their spins will add up to zero. The charged lepton will carry the spin of the τ^- lepton, and it is preferentially emitted against the direction of τ^- lepton spin.

In the decay $\tau^- \to \pi^-\nu$, there is zero orbital momentum in the two-body τ^- lepton decay and, since the pion carries no spin, angular momentum conservation requires the neutrino

JHEP01(2024)101

to carry the spin of the τ^- lepton. In the τ^- lepton rest frame, the neutrino and pion are emitted back-to-back. Since the neutrino is always left-handed, the π^- prefers small values for the angle θ in the decay of a right-handed τ^- lepton (τ^-_R) and large values in case the τ^- lepton is left-handed (τ^-_L). In this case, the angle θ carries full spin information.

The decay into a spin-one resonance, ρ or a_1, also offers the simplicity of a two-body decay, like the $\tau^- \to \pi^-\nu$ decay, but with more complicated dynamics since the ρ and a_1 resonances can have longitudinal and transverse polarization. Conservation of angular momentum allows the ρ and a_1 helicities to be equal to $\lambda_V = 0$ or -1.

If the τ^- lepton is in the right-handed state, the V ($V = \rho, a_1$) resonance tends to be in a longitudinally polarized state ($\lambda_V = 0$). Conversely, if the τ^- lepton is left-handed, the V is preferably transversely polarized ($\lambda_V = -1$). Combining the spin amplitudes for all possible configurations of the V resonance and τ^- lepton helicities, one gets [37]:

$$\frac{1}{\Gamma}\frac{d\Gamma}{d\cos\theta} \propto 1 + \alpha_V \lambda_\tau \cos\theta, \tag{7.2}$$

where the dilution factor $\alpha_V = (|\mathcal{M}_L|^2 - |\mathcal{M}_T|^2)/(|\mathcal{M}_T|^2 + |\mathcal{M}_L|^2) = (m_\tau^2 - 2\,m_V^2)/(m_\tau^2 + 2\,m_V^2)$ is a result of the presence of the transverse amplitude $\mathcal{M}_T$ of the V resonance in addition to the longitudinal amplitude $\mathcal{M}_L$. The value of the factor α_V characterizes the sensitivity of the $\cos\theta$ observable. For comparison, in the τ^- lepton decay to the a_1 resonance, $\alpha_{a_1} = 0.021$, in the ρ meson decay, $\alpha_\rho = 0.46$ and in the pion decay, $\alpha_\pi = 1$. Consequently, the sensitivity to the τ^- lepton helicity in $\tau \to V\nu$ decays is strongly reduced if only the angle θ is considered.

The spin of V is transformed into the total angular momentum of the decay products and thus can be retrieved by analyzing the subsequent V decay.

There are two additional angles to be considered in the decay of $\tau^- \to \rho^-\nu$ followed by $\rho^- \to \pi^-\pi^0$: the angle β denotes the angle between the direction of the charged pion in the ρ meson rest frame and the direction of the ρ meson momentum, given by:

$$\cos\beta = \vec{n}_{h^\pm} \cdot \vec{n}_\rho = \frac{m_\rho}{\sqrt{m_\rho^2 - 4m_\pi^2}} \frac{E_{\pi^-} - E_{\pi^0}}{|p_{\pi^-} - p_{\pi^0}|}, \tag{7.3}$$

where $\vec{n}_{h^\pm}$ is a unit vector along the direction of the charged pion in the ρ meson rest frame and $\vec{n}_\rho$ is the direction of the momentum of the ρ projected onto its rest frame. The rotation plane of two pions is aligned correspondingly to the spin of the ρ resonance. In the case of $\lambda_\rho = 0$, the angle β tends to small values, and to large values if $\lambda_\rho = -1$. The angle β in $\tau^- \to \rho^-\nu$ is sketched in figure 3b. The expression 7.3 for this angle contains only quantities that can be measured directly and is therefore a very powerful variable to discriminate left- and right-handed helicity states.

A similar, but not identical, angle β is constructed for the $\tau^- \to a_1^-\nu$. In this case β is defined as the angle between the normal to the 3π decay plane and the a_1 meson momentum vector projected onto the a_1 meson rest frame. The angle is shown in figure 3c.

A further angle α is defined by the two planes spanned by vectors $(\vec{n}_V, \vec{n}_\tau)$ and $(\vec{n}_V, \vec{n}_{h^\pm})$, respectively:

$$\cos\alpha = \frac{(\vec{n}_V \times \vec{n}_\tau) \cdot (\vec{n}_V \times \vec{n}_{h^\pm})}{|\vec{n}_V \times \vec{n}_\tau||\vec{n}_V \times \vec{n}_{h^\pm}|}. \tag{7.4}$$

JHEP01(2024)101

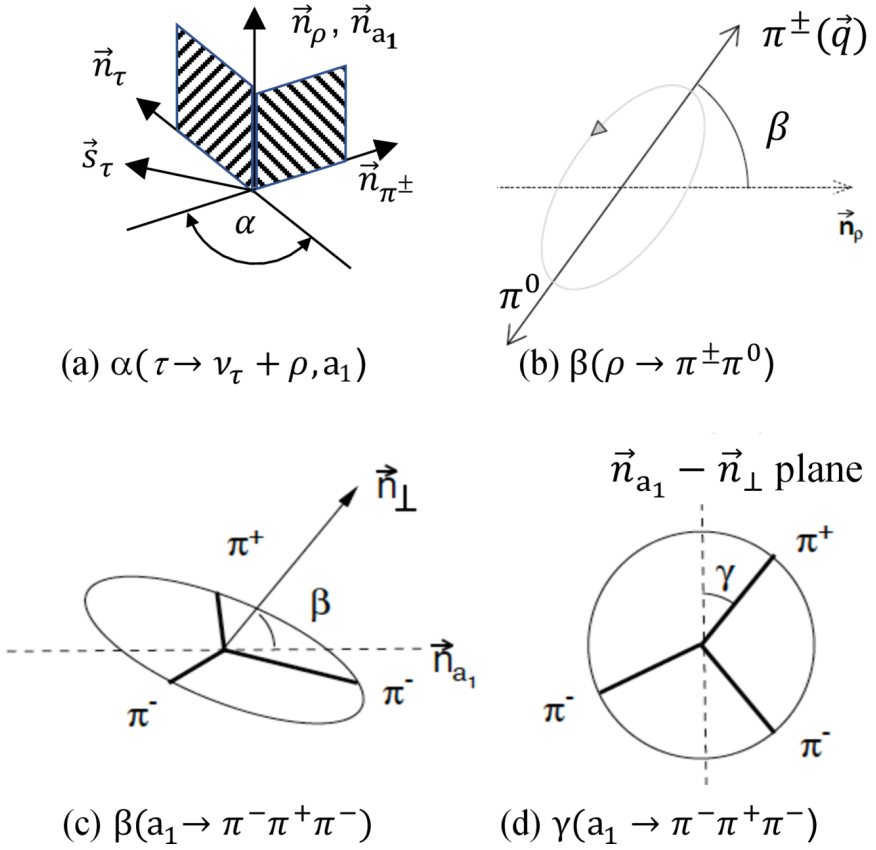

Figure 3. Definitions of (a) the angle α in both $\tau^- \to \rho^-\nu$ and $\tau^- \to a_1^-\nu$, (b) the angle β in $\tau^- \to \rho^-\nu, \rho^- \to \pi^-\pi^0$ and (c) in $\tau^- \to a_1^-\nu, a_1^- \to \pi^-\pi^+\pi^-$, and finally (d) the angle γ for the decay of $a_1^- \to \pi^-\pi^+\pi^-$. Figures b, c, and d have been taken and refurbished from ref. [38].

Here, all vectors are defined in the resonance rest frame. The vector $\vec{n}_V$ denotes the boost direction of the ρ or a_1 resonance projected onto its rest frame, and $\vec{n}_\tau$ is the boost direction of the τ^- lepton in the rest frame of the meson. The vector $\vec{n}_{h^\pm}$ denotes the momentum direction of the π^- in case of $\tau^- \to \rho^-\nu$ decay and π^+ in $\tau^- \to a_1^-\nu$ decay. The angle α describes the correlation between the helicity of the τ lepton and the decay products of the ρ or a_1 resonance. The angle α is illustrated in figure 3a.

An additional angle γ can be introduced in the $\tau^- \to a_1^-\nu$ decay; the angle describes the relative orientation of the pions in the decay plane. This angle is illustrated also in figure 3d. All spin sensitive angles α, β, γ and θ can be combined into a unique one-dimensional variable, without loss of sensitivity, as described in the next section.

7.2 Optimal observables

Optimal variables to measure the helicity of τ^- leptons have been widely explored at LEP and are explained in ref. [39]. The idea is to replace the multidimensional fits over all relevant decay angles by a one dimensional fit to a unique variable $\omega(\theta, \alpha, \beta, \gamma, \ldots)$, which can be derived from the squared matrix elements of the decay for positive and negative helicity. This procedure is equivalent to the use of the concept of the polarimetric vector.

JHEP01(2024)101

In general, the differential width of any decay of a polarized τ^- lepton can be described using the polarimetric vector and has the simplified form [15, 37, 38]:

$$\mathrm{d}\Gamma = \frac{|\overline{\mathcal{M}}|^2}{2m_\tau}(1 - h_\mu s^\mu)\mathrm{d}S, \tag{7.5}$$

where $\mathrm{d}S$ is the element of Lorentz-invariant phase space, s is the four-vector of the spin of the τ^- lepton and h is the polarimetric four-vector. In the rest frame of the τ^- lepton, assuming that the τ^- lepton spin is aligned with the τ^- lepton momentum (all transverse τ^- spin components are zero), this reads:

$$\frac{\mathrm{d}\Gamma}{\mathrm{d}\cos\zeta_h} \propto \frac{1}{2}(1 + \mathcal{P}_\tau \cos\zeta_h), \tag{7.6}$$

where $\mathcal{P}_\tau$ is the τ^- lepton polarization for a given τ^- lepton decay and ζ_h is the angle between the space-like polarimetric vector $\vec{h}_\tau$ and $\vec{n}_\tau$, the direction of the τ^- lepton as defined above.

The polarimetric vector $\vec{h}_\tau$ depends on the particular final state. This vector describes how the tau decay products propagate depending on the tau spin; for τ^- lepton decays into hadrons it depends on the momenta of all the hadrons in the decay chain and the decay mode of the intermediate resonance.

In the case of $\tau^- \to \pi^-\nu$, the polarimetric vector is aligned with the direction of the π^- meson: $\vec{h}_\tau = \vec{n}_\pi$, where $\vec{n}_\pi$ is a unit vector pointing along the momentum of the pion.

The situation in $\tau^- \to (\rho^- \to \pi^-\pi^0)\nu$ and $\tau^- \to (a_1^- \to \pi^-\pi^+\pi^-)\nu$ decays is more complicated due to the resonance structure. The general expressions for polarimetric vectors in the decays $\tau^- \to \rho^-\nu$ and $\tau^- \to a_1^-\nu$ is reported in ref. [38] and references therein, including a discussion of the hadronic form factor in $\tau^- \to a_1^-\nu$ decays.

We denote the optimal observable for a single τ^- lepton decay as $\omega(\mathrm{h})$, which is defined in ref. [39]:

$$\omega(\mathrm{h}) = \cos\zeta_h. \tag{7.7}$$

The optimal observable $\omega(\mathrm{h})$ carries the full sensitivity and has the same unique distribution distinguishing left and right τ lepton helicities for all hadronic decay modes. The simple linear distribution of $\omega(\mathrm{h})$ (for $\mathrm{h} = \pi, \rho, a_1$) is shown in figure 5 of ref. [38]. The use of such an optimal variable simplifies the extraction of the polarization and combines all spin sensitive angles, even those with low discrimination power, into a one-dimensional quantity.

For the $\tau^- \to a_1^-\nu$ decay, we use the parametrization provided by the CLEO Collaboration [40] for the hadronic form factor, which includes in total seven resonances that describe the intermediate states of the $a_1^- \to \pi^-\pi^+\pi^-$ decay. The CLEO parametrization for this decay mode is also used in the TAUOLA [15, 16] and PYTHIA 8 [13] Monte Carlo generators.

7.3 Helicity correlations

The sensitivity to the polarization measurement can be improved by exploiting the anti-correlation of helicity within a τ lepton pair. The method, proposed in ref. [39], defines a

JHEP01(2024)101

Channel	Category	Discriminator	
$\tau_e\tau_\mu$	$e + \mu$	$m_{vis}(e, \mu)$	visible mass
$\tau_e\tau_h$	$e + a_1$	$\omega(a_1)$	optimal observable with SVFIT
	$e + \rho$	$\omega_{vis}(\rho)$	visible optimal observable
	$e + \pi$	$\omega(\pi)$	optimal observable with SVFIT
$\tau_\mu\tau_h$	$\mu + a_1$	$\omega(a_1)$	optimal observable with SVFIT
	$\mu + \rho$	$\omega_{vis}(\rho)$	visible optimal observable
	$\mu + \pi$	$\omega(\pi)$	optimal observable with SVFIT
$\tau_h\tau_h$	$a_1 + a_1$	$m_{vis}(a_1, a_1)$	visible mass
	$a_1 + \pi$	$\Omega(a_1, \pi)$	combined optimal observable with SVFIT
	$\rho + \tau_h$	$\omega_{vis}(\rho)$	visible optimal observable (for leading ρ)
	$\pi + \pi$	$m_{vis}(\pi, \pi)$	visible mass

Table 2. Final choice of discriminators in the various event categories.

new optimal observable for the τ lepton pair. Denoting ω_1 and ω_2 to be the observables for τ_1 and τ_2, one can define the variable:

$$\Omega = \frac{\omega_1 + \omega_2}{1 + \omega_1\omega_2}. \tag{7.8}$$

Similarly to the optimal observable for a single τ decay, the distribution of Ω for a τ pair is identical for all hadronic decay modes, as shown in figure 6 in ref. [38].

7.4 Reconstruction of $\omega(h)$ and the choice of discriminators

The performance of the kinematical reconstruction of τ lepton decays and the polarization observables strongly depends on the decay mode. Therefore, sensitivity is improved by treating separately each decay mode, which results in 11 categories in the $\tau_e\tau_\mu$, $\tau_e\tau_h$, $\tau_\mu\tau_h$, and $\tau_h\tau_h$ channels. These categories are summarized in the first two columns of table 2. In the fully hadronic channel, the three combinations containing $\tau^- \to \rho^-\nu$ events are combined into one category for the choice of the optimal discriminator.

The reconstruction of the optimal observables $\omega(h)$ requires the knowledge of the rest frame of the τ lepton or of both τ leptons for the calculation of the quantity Ω. Because of the emission of the neutrino, the momentum direction of τ leptons can be measured directly only in cases where the decay vertex can be reconstructed, for example for decays like $\tau^- \to \pi^-\pi^+\pi^-\nu$. In most other cases, the SVFIT [41] algorithm for the reconstruction of the τ lepton decay is used. The SVFIT algorithm has been modified for the purpose of this analysis, such that:

- the four-vector of individual τ leptons is calculated by SVFIT;
- the mass of the di-τ system is constrained to the Z boson mass to improve the resolution on the four-vectors of the two τ leptons;

JHEP01(2024)101

The reconstructed τ^- lepton four-vectors are used to boost the four-vectors of the τ^- decay products to the τ^- lepton rest frame and to compute the optimal observable $\omega(h)$ in the τ^- lepton rest frame.

Since the performance of the SVFIT algorithm is limited, in some event categories a better sensitivity is often obtained from observables that are measured directly in the detector, e.g., the angle β in ρ decays, and the angles β and γ in $\tau^- \to a_1^-\nu$ decays, as defined by eq. (7.3). These quantities are denoted hereafter in the text as visible observables ω_{vis} or Ω_{vis}.

In addition, it has been shown in ref. [42] that the energies of the τ lepton decay products and the acollinearity angle between the decay products of the two τ leptons in the laboratory frame also carry information about the helicity states of the τ leptons. A suitable observable, which includes both quantities, is the invariant mass of the visible decay products of both τ leptons

$$m_{vis} = \sqrt{2E_1E_2(1 - \cos\varphi(\tau_1^{vis}, \tau_2^{vis}))}, \tag{7.9}$$

where E_1 and E_2 are the energies of the detected leptons and hadrons in the final states of τ_1 and τ_2 and $\varphi(\tau_1^{vis}, \tau_2^{vis})$ the acollinearity angle defined as the angle between the decay products of the two τ leptons. The visible mass m_{vis} is used for $e^\pm + \mu^\mp$, $\pi^+ + \pi^-$, and $a_1^+ + a_1^-$ pairs.

The decision of which observable to use in each category was made on the basis of a likelihood scan of the expected sensitivity in each category with the simulated data sample. All possible observables were evaluated for each category. The result of the best choice is given in the last column of table 2. For the category $(\rho + \tau_h)$ we use $\omega_{vis}(\rho) = \cos\beta$ for all possible decays of τ_h, and for the combination where both τ leptons decay via a ρ we use $\omega_{vis}(\rho)$ of the ρ with the highest p_T.

8 Systematic uncertainties

The estimated systematic uncertainties follow closely the analysis of ref. [35] and an earlier analysis that uses the same data set [19]. Our uncertainties are briefly discussed in the following, indicating differences and refinements compared with previous analyses. Systematic uncertainties are modeled as nuisance parameters with log-normal (gaussian) probability distribution functions for normalization (shape) uncertainties in the maximum likelihood fits described in section 10. This section presents the initial uncertainties used for the nuisance parameters. The systematic uncertainties that affect only the normalization of signal and background processes are summarized in table 3, and those that could alter the distributions of the τ polarization observables are summarized in table 4.

The overall luminosity uncertainty of 1.2% has been determined in ref. [11]. The uncertainty in the Drell-Yan cross section is a combination of the uncertainty in the theoretical cross section and PDF, α_s, and QCD scale variations were evaluated in ref. [19]. The uncertainties for $t\bar{t}$ (4.2%), diboson (5%), and EWK cross sections (4%) were established in ref. [19]. The normalization of the W+jets cross section is different for various channels due to the different contributions and methods; in the $\tau_e\tau_\mu$ channel a MC simulation was used, whereas in the $\tau_e\tau_h$ and $\tau_\mu\tau_h$ channels the *ABCD* method was used as described in section 6. For the $\tau_h\tau_h$ channel the W+jets contribution is very small and only the cross

JHEP01(2024)101

Source of uncertainty	Initial uncertainties per channel			
	$\tau_h\tau_h$	$\tau_\mu\tau_h$	$\tau_e\tau_h$	$\tau_e\tau_\mu$
Integrated luminosity	1.2%	1.2%	1.2%	1.2%
DY cross section	5.6%	5.6%	5.6%	5.6%
$t\bar{t}$ cross section	4.2%	4.2%	4.2%	4.2%
Diboson cross section	5%	5%	5%	5%
EWK cross sections	4%	4%	4%	4%
W+jets cross section & normalization	4%	10%	10%	20%
QCD bkg. normalization	3%	20%	20%	10%
b-tagging efficiency	$\leq$0.1% except for $t\bar{t}$ and VV(1–9%)			
e identification efficiency (*correlated*)	—	—	2%	2%
e tracking efficiency (*correlated*)	—	—	1%	1%
μ identification efficiency (*correlated*)	—	2%	—	2%

Table 3. Systematic uncertainties affecting only the normalization of templates. The table lists the estimated inital uncertainties used in the fit for these nuisance parameters. The label *correlated* means that these uncertainties are common to the respective channels.

section uncertainty is applied. For the QCD normalization uncertainty we assign: (i) 10% uncertainty for the $\tau_e\tau_\mu$ channel; (ii) 20% for the $\tau_e\tau_h$ and $\tau_\mu\tau_h$ channels because of an extrapolation uncertainty from the loose isolation control region; and (iii) 3% for the $\tau_h\tau_h$ channel because we use a data driven method, see section 6.2. The b quark tagging efficiency uncertainty is applied only for the $t\bar{t}$ and diboson processes.

The e and μ identification efficiency uncertainties are 2% and identical for the channels where electrons or muons are used [19]. The muon tracking efficiency is included in the identification efficiency.

The uncertainties listed in table 4 can possibly alter the shape of observables: the electron and muon misidentifications depend on the decay modes and lead to rate uncertainties of 12 and 25% for electron and muon misidentification, respectively; the uncertainty in the jet $\rightarrow \tau_h$ misidentification rate is p_T dependent but does not exceed 40% [19].

The uncertainties in the efficiency of the electron and muon trigger are in the order of 2%, but slightly p_T and η dependent. The muon momentum scale uncertainty is specified in three bins in η and ranges from 0.4 to 2.7%. The hadronic τ momentum scale uncertainty is p_T and decay mode dependent but less than 2% [19]. In addition we added a further 2% contribution to account for possible differences in the charged and neutral hadron energy reconstruction.

The identification efficiencies for τ_h candidates depend on working points of the above mentioned MVA used to refine the decay mode identification and have been evaluated in two regions of p_T, below and above 40 GeV as described in ref. [35]. Similarly the τ_h trigger efficiencies have a p_T and MVA dependence of up to 10% [19]. The same working points are used in the $\tau_\mu\tau_h$ and $\tau_h\tau_h$ channels and are therefore correlated between these two channels. The $\tau_e\tau_h$ channel uses only the electron trigger and therefore is not sensitive to the τ trigger uncertainty.

JHEP01(2024)101

Source of uncertainty	Initial uncertainties per channel			
	$\tau_h\tau_h$	$\tau_\mu\tau_h$	$\tau_e\tau_h$	$\tau_e\tau_\mu$
$e \to \tau_h$ misidentification rate	12% DM dependent			—
$\mu \to \tau_h$ misidentification rate	25% DM dependent			—
jet $\to \tau_h$ misidentification rate	$20\% \times p_T^{jet}/100\,\text{GeV} \leq 40\%$			—
Electron trigger efficiency	—	—	p_T, η dependent $\leq 2\%$	
Electron momentum scale	—	—	Event-dependent	
Electron to tau misid energy scale	—	—	0.8–6.6%	—
Muon trigger efficiency	—	p_T, η dependent $\leq 2\%$	—	p_T $\eta \leq 2\%$
Muon momentum scale	—	0.4–2.7%	—	0.4–2.7 %
Muon to tau misid momentum scale	—	1%	—	—
Hadronic tau momentum scale	p_T & DM dependent $\leq 2\%$			—
Neutral, charged hadrons energy	2%	2%	2%	—
Tau identification efficiency	p_T & DM dependent 2–3%			—
Tau trigger efficiency	p_T & DM dependent $\leq 10\%$		—	—
Misidentified DM $\tau_h \to h^\pm$	2.8%	2.8%	2.8%	—
Misidentified DM $\tau_h \to h^\pm\pi^0$	3.2%	3.2%	3.2%	—
Misidentified DM $\tau_h \to h^\pm h^\mp h^\pm$	3.7%	3.7%	3.7%	—
Drell-Yan MC reweighting	$\leq$100% for all channels			
Top p_T reweighting	$\leq$100% for all channels			
Parton reweighting	$\leq$100% for all channels			
p_T^{miss} unclustered scale	Event-dependent			
p_T^{miss} recoil correction	Event-dependent			
Limited amount of MC events	Bin-by-bin fluctuations			

Table 4. Systematic uncertainties affecting the shapes of templates. The table lists the estimated initial uncertainties used in the fit for these nuisance parameters and their dependencies on p_T, decay mode (DM) or event selection. The comment "Event-dependent" for the p_T^{miss} entries indicates that these corrections vary on an event-by-event basis due to the event selection.

Uncertainties related to the reconstruction of hadronically decaying τ leptons are considered to be uncorrelated between event categories for different decay modes. The imperfect knowledge of the decay mode of the reconstructed, hadronically decaying τ leptons and its uncertainty is a major systematic limitation in this analysis, but can be controlled by the shape of the τ lepton mass for a given decay channel, which includes its contribution from wrongly classified decay modes. Maximum likelihood fits to the τ lepton mass distribution in data obtained normalization factors for these contributions identical to the values of the simulation except for the $\rho + X$ category, where decays containing additional, but not identified, π^0s contribute. A shift of 3.2% corresponding to about one standard deviation of the parameter describing this migration was necessary to make the τ lepton mass distribution agree with data for this decay mode. Table 4 lists the uncertainties of the parameters describing the migration for three important decay modes. For the extraction of the polarization, this

JHEP01(2024)101

correction of the migration has been applied in the $\mu + \rho$ channel, where the visible optimal observable $\omega_{\text{vis}}(\rho)$ is exploited. The effect on the distributions of the τ lepton polarization observables is estimated by varying contributions from events with misidentified hadronic decay modes symmetrically by one standard deviation.

As pointed out in section 7.2, the polarimetric vector in $\tau^- \to \pi^-\nu$ and $\tau^- \to \rho^-\nu$ decays is determined purely by the Lorentz structure of these decays and thus contains no QCD dynamics. The τ lepton decay to three pions and a neutrino is dominated by the $a_1(1260)$ ($J^{PG} = 1^{+-}$) resonance, which decays through the intermediate state of $(\rho\pi)$, with mostly $\rho(770)$ and an admixture of $\rho(1450)$ at higher masses, followed by a $\rho^- \to \pi^-\pi^0$ decay. Theoretical systematic uncertainties originating from the imperfect knowledge of the $a_1 \to 3\pi$ decay substructure have been studied in ref. [38]. The uncertainty in the τ lepton polarization in the a_1 channel due to the variation of resonance parameters is $(\Delta\mathcal{P}_\tau)_{\text{model}} = (1.41 \pm 1.37) \times 10^{-4}$, far below any currently reachable experimental precision and hence neglected.

As described in section 3, the DY MC has been reweighted in p_{T} and rapidity and a variation of 100% of this correction is used to evaluate the systematic effect. The same procedure has been applied to the parton reweighting corrections described in the same section.

The missing unclustered energy uncertainty is applied for $t\bar{t}$ and diboson processes and the $p_{\text{T}}^{\text{miss}}$ recoil correction is varied within the limits determined during the computation of the correction.

A further important contribution to the overall systematic uncertainty arises from the limited amount of MC data, which contributes to bin-to-bin fluctuations.

9 Measurement of the τ lepton polarization

The average τ lepton polarization $\langle\mathcal{P}_\tau\rangle$ is defined as

$$\langle\mathcal{P}_\tau\rangle = \frac{N(\text{Z} \to \tau_{\text{R}}^-\tau_{\text{L}}^+) - N(\text{Z} \to \tau_{\text{L}}^-\tau_{\text{R}}^+)}{N(\text{Z} \to \tau_{\text{R}}^-\tau_{\text{L}}^+) + N(\text{Z} \to \tau_{\text{L}}^-\tau_{\text{R}}^+)}, \tag{9.1}$$

where $N(\text{Z} \to \tau_{\text{R}}^-\tau_{\text{L}}^+)$ and $N(\text{Z} \to \tau_{\text{L}}^-\tau_{\text{R}}^+)$ are the numbers of Z boson decays into τ leptons with positive and negative τ^- lepton helicity, respectively. The average polarization depends on the accepted mass range of the τ lepton pair. The numbers $\text{Z} \to \tau_{\text{L/R}}^-\tau_{\text{R/L}}^+$ are obtained by a maximum likelihood fit of representative templates to the distributions of the observables listed in table 2. The signal templates are derived from simulated signal events. The background templates are composed of the contributions estimated from data or from simulation, as described in section 6.

The extracted numbers from these maximum likelihood fits and thus the polarization are always an average over a range of intrinsic polarization given by

$$\mathcal{P}_\tau = \mathcal{P}_\tau\left(\sin^2\theta_{\text{W}}^{\text{eff}}, \hat{s}, \text{q}\right), \tag{9.2}$$

which depends on the effective weak mixing angle, the quark-antiquark center-of-mass energy $\sqrt{\hat{s}}$ and the quark type q specifying whether the Z boson has been produced via a pair of up- or down-type quarks.

JHEP01(2024)101

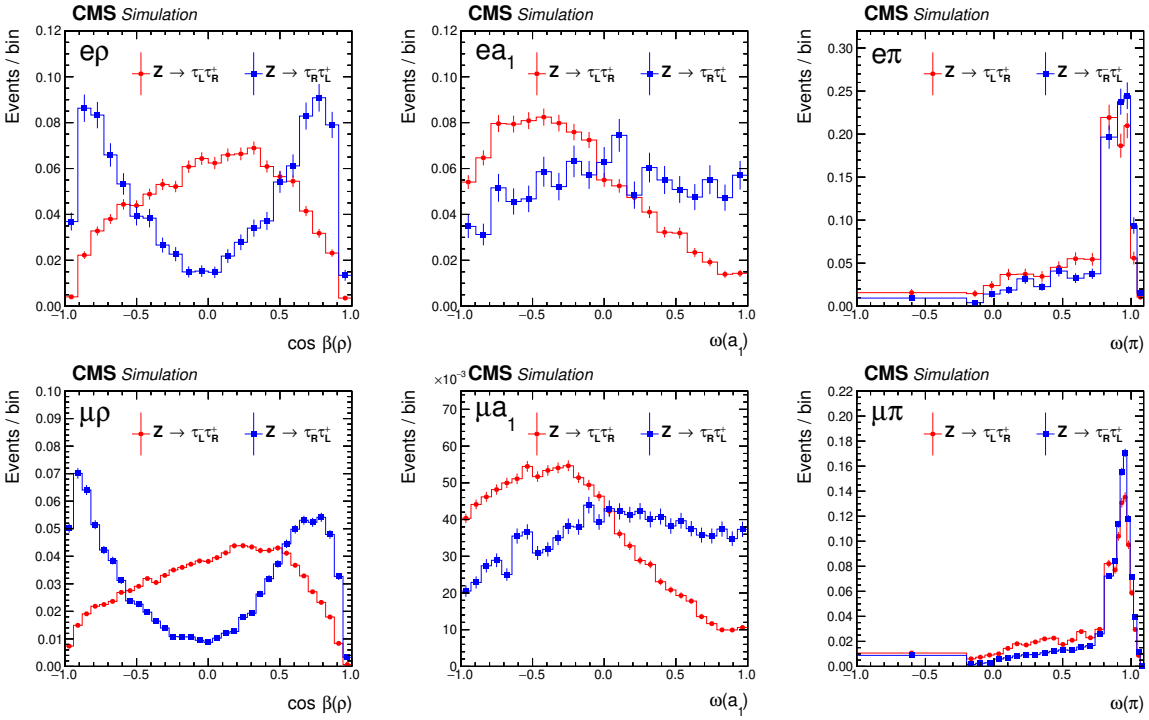

Figure 4. Some examples of templates for six τ^- lepton decays: $e + \rho, e + a_1, e + \pi$ in the upper row and $\mu + \rho, \mu + a_1, \mu + \pi$ in the lower row. The blue and red lines indicate right and left-handed τ^- leptons, respectively. The templates have been rescaled to correspond to zero polarization at the generator level. The uncertainty bars are statistical only and correspond to the limited MC samples after all selections. The shapes of the templates depend on the decay mode and on the nature of the chosen discriminating observables.

The measured average polarization can be written as

$$\left\langle \mathcal{P}_\tau(\sin^2\theta_{\mathrm{W}}^{\mathrm{eff}}) \right\rangle = \frac{\sum_{\mathrm{q=u,d}} \int \mathrm{d}\hat{s}\, \mathcal{P}_\tau\left(\sin^2\theta_{\mathrm{W}}^{\mathrm{eff}}, \hat{s}, \mathrm{q}\right) w\left(\sin^2\theta_{\mathrm{W}}^{\mathrm{eff}}, \hat{s}, \mathrm{q}\right)}{\sum_{\mathrm{q=u,d}} \int \mathrm{d}\hat{s}\, w\left(\sin^2\theta_{\mathrm{W}}^{\mathrm{eff}}, \hat{s}, \mathrm{q}\right)}. \tag{9.3}$$

Here $w\left(\sin^2\theta_{\mathrm{W}}^{\mathrm{eff}}, \hat{s}, \mathrm{q}\right)$ denotes the weights in the averaging. These weights include two effects: (i) the dependence of the cross section σ on the quark-antiquark squared center-of-mass energy $\hat{s}$ and the quark type q for a given value of the mixing angle $\sin^2\theta_{\mathrm{W}}^{\mathrm{eff}}$; and (ii) the acceptance of the detector and the selection efficiency in the analysis, which both depend on $\hat{s}$ and quark q as well.

The efficiencies for right- and left-handed τ^- leptons are different and depend strongly on the decay mode and the selection applied in the analysis, especially on transverse momenta of the τ^- lepton decay products. Therefore, we adopt a method where these effects are included by using templates for right- and left-handed τ^- leptons. The templates are histograms of the τ^- polarization observables for each decay category of the τ^- lepton. They are generated by applying all selections and corrections of the analysis chain to the simulated events of the signal. Generator-level information is used to construct separate templates for right- and left-handed τ^- leptons.

JHEP01(2024)101

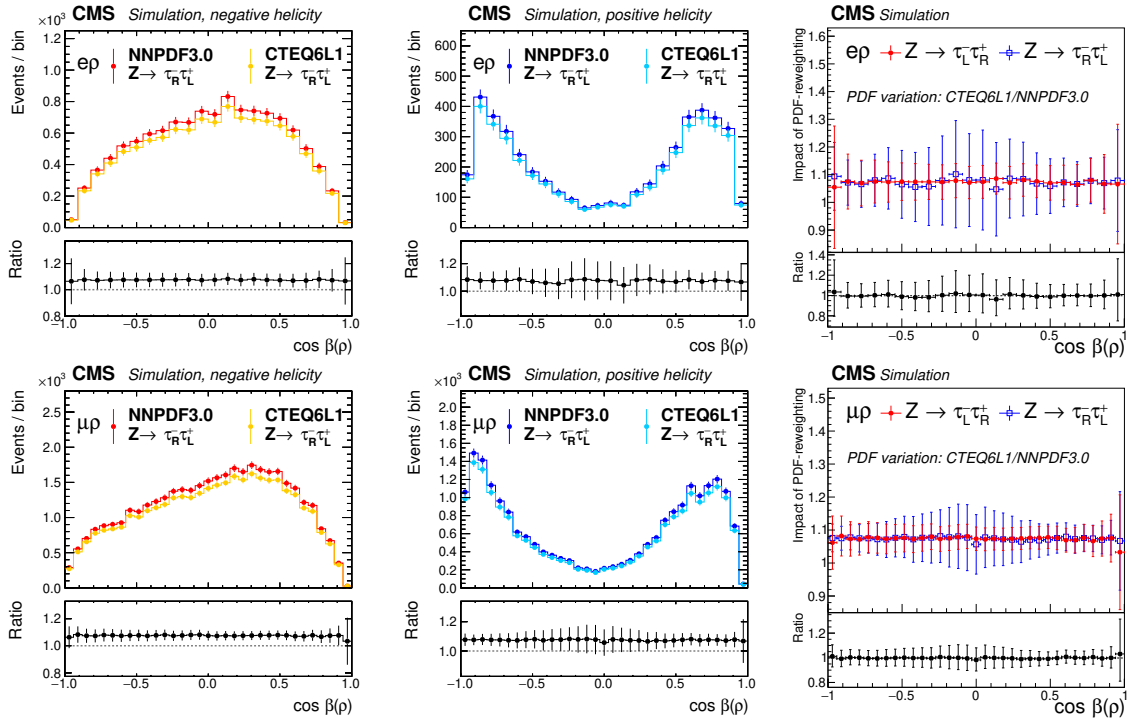

Figure 5. Variation of the templates for negative (left) and positive (middle) τ^- lepton helicities in the $e + \rho$ (upper row) and $\mu + \rho$ (lower row) channels after a change of the PDFs from NNPDF3.0 to CTEQ6L1. The graphs on the right show the ratio of the ratios of the changes for negative and positive helicities, which is flat and centered exactly at 1 demonstrating that a possible PDF effect on the polarization is very small. The drawn error bars are large because the events in the ratios are correlated, so only the fluctuations of the points are relevant and are within approximately 1%, much smaller than other systematic uncertainties in this analysis.

These templates are normalized such that they correspond to zero polarization for a given range (75–120 GeV) of $\sqrt{\hat{s}}$ at the generator level. The normalization proceeds in the following way. First the templates are defined using the simulated data samples described above for signal and background:

$$\mathcal{T}(\text{simulation}) = \mathcal{T}(\text{sig.}, \langle \mathcal{P}_\tau \rangle, r) + \mathcal{T}(\text{bkg.}). \tag{9.4}$$

The signal template $\mathcal{T}(\text{sig.}, \langle \mathcal{P}_\tau \rangle, r)$ contains the two parts $\mathcal{T}(\text{Z} \to \tau_\text{R}^- \tau_\text{L}^+)$ and $\mathcal{T}(\text{Z} \to \tau_\text{L}^- \tau_\text{R}^+)$ for the two helicity states and depends on two parameters of interest, the average τ polarization $\langle \mathcal{P}_\tau \rangle$ and an overall signal strength modifier r as given in the following equation,

$$\mathcal{T}(\text{sig.}, \langle \mathcal{P}_\tau \rangle, r) = r \left[\frac{1 + \langle \mathcal{P}_\tau \rangle}{2} \mathcal{T}(\text{Z} \to \tau_\text{R}^- \tau_\text{L}^+) + \frac{1 - \langle \mathcal{P}_\tau \rangle}{2} \mathcal{T}(\text{Z} \to \tau_\text{L}^- \tau_\text{R}^+) \right]. \tag{9.5}$$

To extract the average τ^- lepton polarization directly from the fit, the signal templates entering the fit must be rescaled such that they correspond to an unpolarized sample of $\text{Z} \to \tau^+ \tau^-$ events. This is achieved by renormalizing the integrals of the templates $\mathcal{T}(\text{Z} \to \tau_\text{L/R}^- \tau_\text{R/L}^+)$

JHEP01(2024)101

with the product of two factors, $s_{\mathrm{LR/RL}}$ and s_{tot}, where

$$s_{\mathrm{LR/RL}} = \frac{1}{N_{\mathrm{gen}}(\mathrm{Z} \to \tau^{-}_{\mathrm{L/R}}\tau^{+}_{\mathrm{R/L}})}, \tag{9.6}$$

$$s_{\mathrm{tot}} = N_{\mathrm{gen}}(\mathrm{Z} \to \tau^{-}_{\mathrm{R}}\tau^{+}_{\mathrm{L}}) + N_{\mathrm{gen}}(\mathrm{Z} \to \tau^{-}_{\mathrm{L}}\tau^{+}_{\mathrm{R}}). \tag{9.7}$$

These normalization factors are obtained from event counts at the generator level for each N_{gen} before any selections are applied. The scale factor $s_{\mathrm{LR/RL}}$ produces an unpolarized sample before the event selection and the second factor s_{tot} ensures that the overall number of signal events remains unchanged. In this way, the templates for right- and left-handed helicities incorporate all biases due to the trigger and analysis selections, and the average polarization can be read off directly from the fit results according to eq. (9.5).

All experimental selections are contained in the templates and all systematic uncertainties discussed in the previous section are applied simultaneously to the signal and background templates in the global maximum likelihood fits presented in section 10. The significance of the specific normalization of the templates means that they refer to a null average polarisation within a mass window of 75 to 120 GeV at the generator level.

A global maximum-likelihood fit is performed in the 11 event categories given in table 2 in the $\tau_{\mathrm{e}}\ \tau_{\mu}$, $\tau_{\mathrm{e}}\ \tau_{\mathrm{h}}$, $\tau_{\mu}\ \tau_{\mathrm{h}}$, and $\tau_{\mathrm{h}}\ \tau_{\mathrm{h}}$ channels. We treat the signal strength r as a free parameter in this fit in order to ensure that only the shape information is used to estimate the average τ lepton polarization $\langle \mathcal{P}_{\tau} \rangle$.

The templates of the two signal contributions $\mathrm{Z} \to \tau^{-}_{\mathrm{L/R}}\tau^{+}_{\mathrm{R/L}}$ reflect the bias from detector acceptance and event selection, and thus the average polarization is retrieved correctly by the fit according to eqs. (9.4) and (9.5).

A closure test using MC simulated events was performed to verify that the procedure for measuring the τ lepton polarization is unbiased.

Representative templates for three of the 11 decay categories are presented in figure 4. The difference in the templates between right- and left-handed τ^{-} leptons is clearly visible. The distinctive shapes in different decay channels are partially distorted by the trigger and analysis selection. This is particularly true for the lepton plus pion channel where the p_{T} selection suppresses the left-hand part of the distribution. From this, it is evident that various categories have different discrimination power. The distributions also demonstrate some bin-by-bin fluctuations that sometimes exceed the statistical fluctuations of the MC samples. Those fluctuations are included when treating the systematic uncertainties, whereas the plots contain only the statistical uncertainties.

To test the stability of the templates with respect to different PDF choices, events are reweighted by the relative weights of 13 different sets of PDFs available for the analysis and new templates are created from the reweighted events. The change in the normalization and shape of the templates was studied with respect to the nominal PDF set (NNPDF3.0), finding that only the overall normalization changes by at most a few percent, whereas the shapes remain unchanged, affecting the templates for positive and negative helicity in the same way, so that the relative ratio between the templates remained constant. In other words, the average polarization extracted from the ratio of templates according to eq. (9.5) does not change.

JHEP01(2024)101

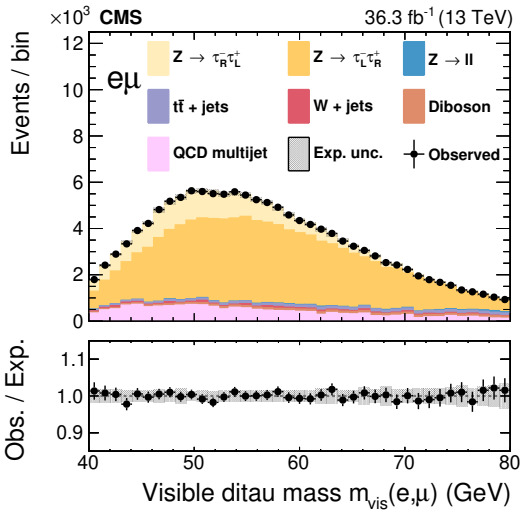

Figure 6. The final maximum likelihood fit of the template to the data for the $\tau_e\tau_\mu$ channel. The figure shows the contributions of all backgrounds and the fitted contributions from τ_L^- and τ_R^- helicity states. The bottom panel of shows the ratio of the experimental data to the sum of the expected contributions. The vertical error bars on the data points are the statistical uncertainties, the gray rectangles indicate the systematic experimental uncertainty in the total expectation.

In figure 5 we compare templates with NNPDF3.0 and CTEQ6L1 PDFs for both negative and positive τ^- lepton helicities in the $e + \rho$ and $\mu + \rho$ categories. The change is uniform and of a few percent, and the double ratio of the relative overall changes is identical to unity for all studied variations and less than 1% on the polarization measurement, as shown by the third graph of figure 5.

A further test of the stability of the procedure consisted in a subdivision of the data into three bins of pseudorapidity of the decaying Z boson: $|\eta|^Z < 1.3$, $1.3 < |\eta^Z| < 2.2$, and $|\eta^Z| > 2.2$. This test was of particular importance to assure that there is no bias in the polarization measurement in different kinematic regions.

10 Results

In this section we present the results of the maximum likelihood fits of the templates to the observed distributions of the chosen discriminators (see table 2), which lead to the extraction of the average polarization. Figures 6, 7, and 8 show how well the data are described by the final maximum likelihood fits for the categories $\tau_e\tau_\mu$, $\tau_e\tau_h$ and $\tau_\mu\tau_h$ combined, and $\tau_h\tau_h$, respectively.

The final results of the average polarization $\langle\mathcal{P}_\tau\rangle_{75\text{–}120\,\text{GeV}}$ obtained by these maximum likelihood fits to data are shown in figure 9. The subscript 75–120 GeV refers to the normalization of the templates as explained in section 9. The highest sensitivity to $\mathcal{P}_\tau$ occurs in the $\mu + \rho$ category, which benefits from more data and an optimal observable ω_{vis} based only on directly measured quantities; the lowest sensitivity occurs in the fully hadronic decay categories, which suffer from high trigger and selection thresholds.

JHEP01(2024)101

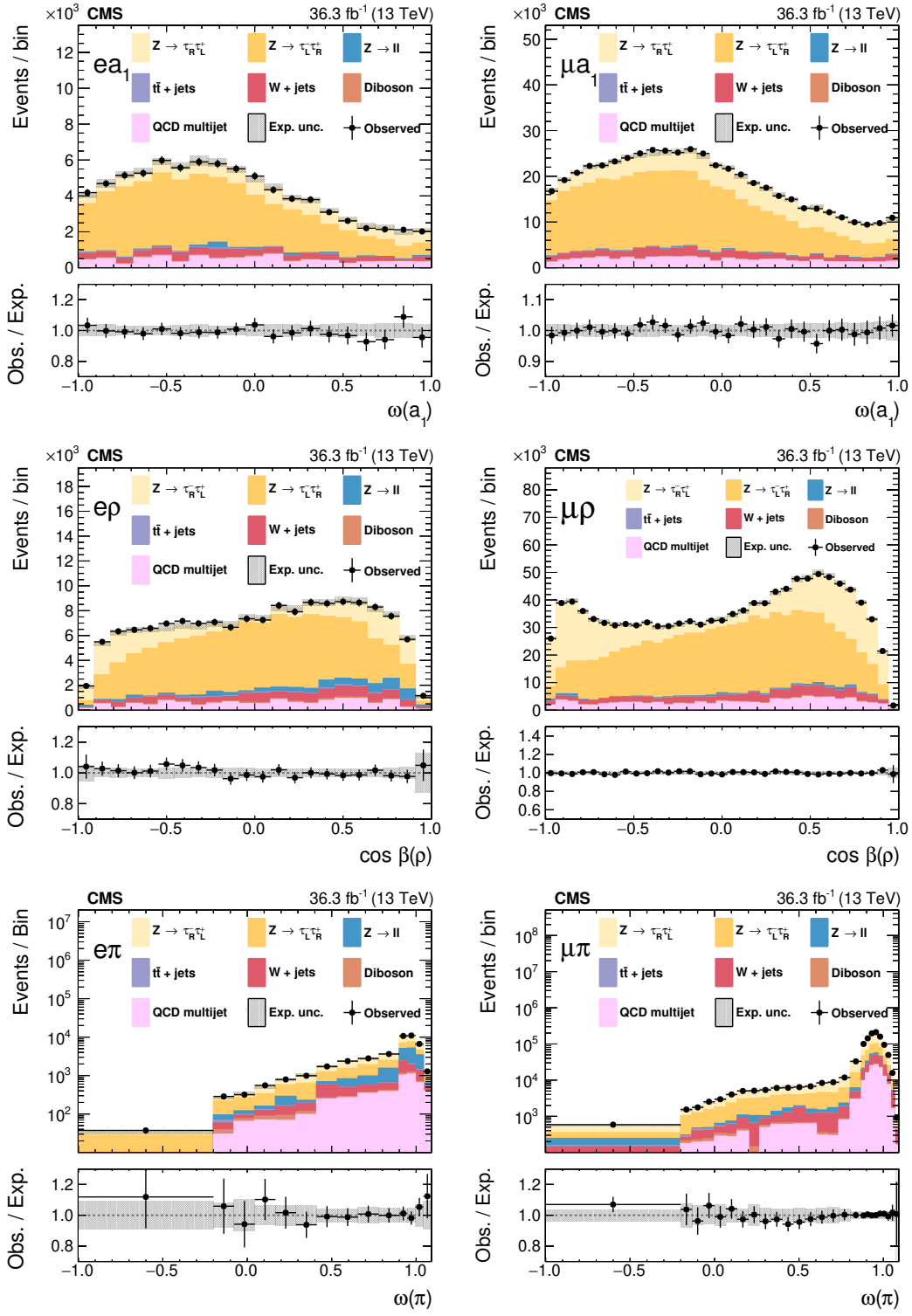

Figure 7. The final maximum likelihood fits of templates to the data for the three $\tau_e\tau_h$ (left) and three $\tau_\mu\tau_h$ (right) categories. The figures show the contributions of all backgrounds and the fitted contributions from τ_L^- and τ_R^- helicity states. The bottom panels show the ratio of the experimental data to the sum of the expected contributions. The vertical error bars on the data points are the statistical uncertainties, the gray rectangles indicate the systematic experimental uncertainty in the total expectation.

JHEP01(2024)101

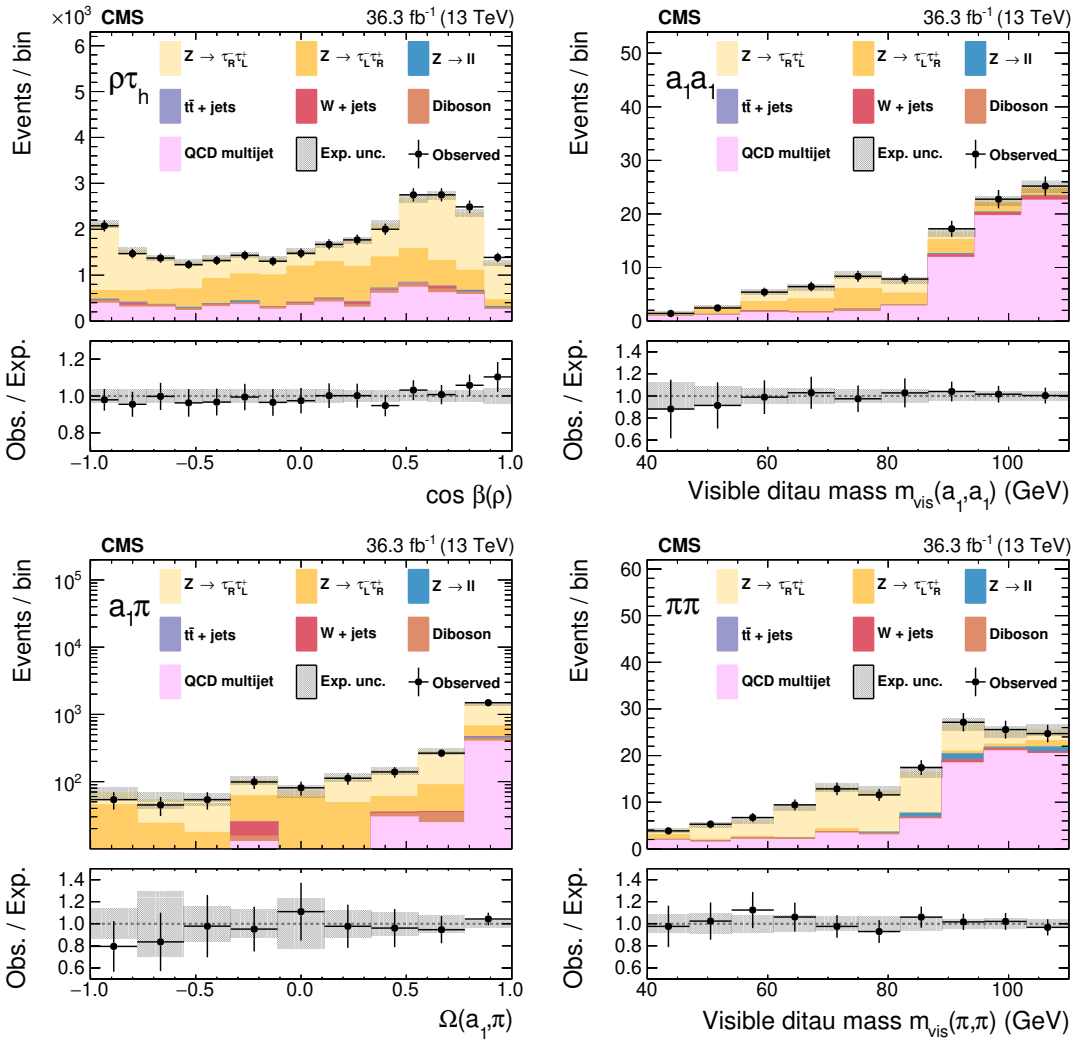

Figure 8. The final maximum likelihood fits of the templates to the data for the $\tau_h\tau_h$ channels. The figures show the contributions of all backgrounds and the fitted contributions from τ_L^- and τ_R^- helicity states. The bottom panels show the ratio of the experimental data to the sum of the expected contributions. The vertical error bars on the data points are the statistical uncertainties, the gray rectangles indicate the systematic experimental uncertainty in the total expectation.

The average τ^- lepton polarization referring to an interval of 75–120 GeV of the generated di-τ mass is:

$$\langle \mathcal{P}_\tau \rangle_{75-120\,\text{GeV}} = -0.140 \pm 0.006\,(\text{stat}) \pm 0.014\,(\text{syst}) = -0.140 \pm 0.015. \tag{10.1}$$

The extracted polarization value is stable with respect to a change of the kinematical region like pseudorapidity. The polarization is evaluated in three different $|\eta^Z|$ bins of the Z boson and the values agree with each other within their uncertainties.

The measurement is limited by systematic uncertainties, predominantly the decay mode migrations that contribute an uncertainty of ±0.008 in the global maximum likelihood fit to the average polarisation. An additional important contribution of ±0.010 originates from

JHEP01(2024)101

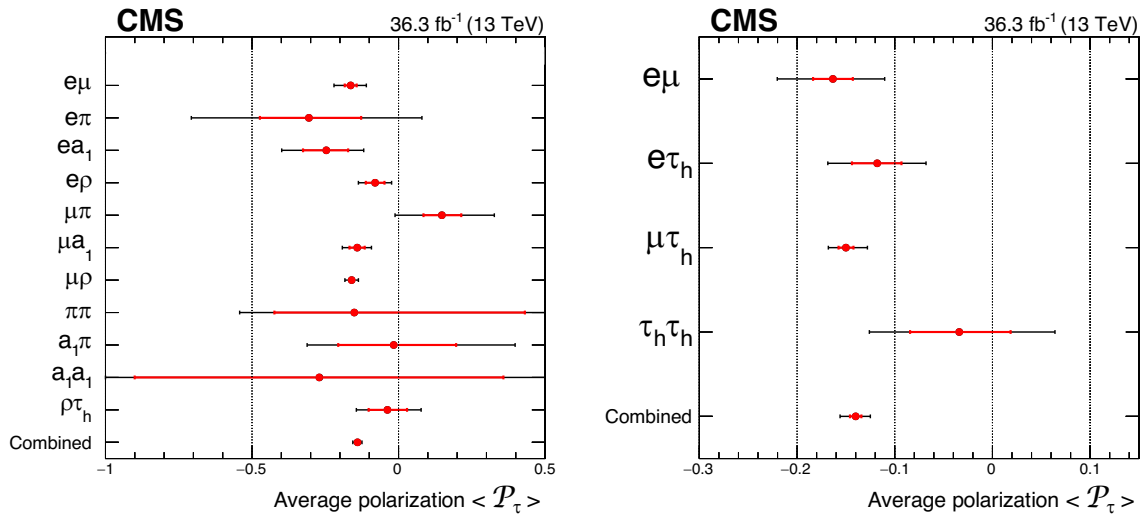

Figure 9. Results of the maximum likelihood fits for the average τ^- lepton polarization for the 11 event categories and the combined fit as the lowest point in the figure on the left. On the right the results for the categories are grouped into 4 channels separately and are shown together with the combined fit. The inner error bars represent the statistical uncertainty, and the outer bars include the systematic uncertainty.

bin-to-bin fluctuations in the signal MC-data. Other sources of uncertainty contribute less than ± 0.005 to the average polarisation.

To compare to previous measurements, such as those at LEP we have to correct the measured average polarization $\langle \mathcal{P}_\tau \rangle$ of the mass interval of 75–120 GeV to the polarization value at the Z pole.

To establish a relation between the average polarization and the value at the Z pole we generated four MadGraph5_aMC@NLO samples of Drell-Yan events at LO in EWK with different values for the weak mixing angle. For each of these samples of 1 million events, we count the number of left- and right-handed τ^- lepton within the interval $75 \leq \sqrt{\hat{s}} \leq 120$ GeV at the generator level. In this way we calculate the average polarization according to its definition, eq. (9.1). We find a constant shift of -0.004 between the average and the peak polarization estimated according to eq. (1.5), independently of the weak mixing angle.

The corrected value of the polarization at the Z pole, which gives directly the negative of the asymmetry parameter A_τ, is then:

$$\mathcal{P}_\tau(\mathrm{Z}) = -A_\tau = -0.144 \pm 0.006\,(\mathrm{stat}) \pm 0.014\,(\mathrm{syst}) = -0.144 \pm 0.015. \qquad (10.2)$$

Figure 10 compares the measured asymmetry parameter A_τ with published results of previous experiments: the four LEP experiments [43], SLD [6] and the combination of LEP and SLD. The earlier result of ATLAS at $\sqrt{s} = 8$ TeV [7], which is also included in the figure is an average over the mass range of 66–116 GeV and was not corrected to the Z pole. The LEP experiments used the ZFITTER package [44] to translate a measured average polarization around the peak of the Z resonance to the asymmetry parameter A_τ. At LEP the average over a small mass interval was due to initial- and final-state photon radiation.

JHEP01(2024)101

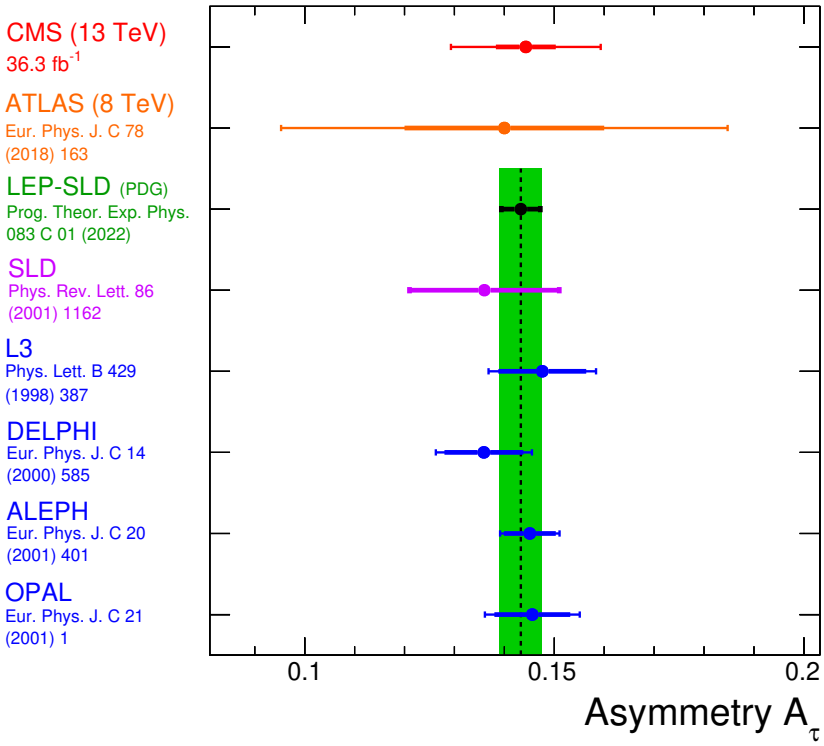

Figure 10. A comparison of the τ^- lepton asymmetry, A_τ measured from the τ^- lepton polarization in this paper and other measurements. The value of A_τ for CMS is obtained based on the Z boson polarization eq. (10.2) and using eq. (1.4). The green band indicates the τ^- lepton polarization value obtained by combining the SLD measurement [6] with the measurements performed at LEP (ALEPH [2], DELPHI [3], L3 [4], and OPAL [5]). The measurement performed by the ATLAS Collaboration at a lower center-of-mass energy of 8 TeV is documented in ref. [7]. The CMS measurement refers to the result of the analysis presented in this paper. The inner horizontal bars represent the statistical uncertainly, the outer bars include the systematic uncertainty.

Their observed shift of the average polarization with respect to the pole value is accidentally of the same size as the correction applied in this analysis. Initial-state gluon radiation of the incoming quarks, which is more important than photon radiation, is included in the MadGraph5_aMC@NLO simulation. No further NLO corrections have been applied to the asymmetry parameter, since it is expected that their effect will be significantly smaller than the systematic uncertainties. It is the most precise measurement of A_τ at the LHC and of comparable precision as the SLD experiment.

The measured asymmetry parameter A_τ by CMS is in good agreement with the LEP average of $A_\tau = 0.1439 \pm 0.0043$ [43] and compatible with the global SM value for the lepton asymmetry parameter assuming lepton universality $A_\ell = 0.1468 \pm 0.0003$ [45]. The tabulated results presented in figures 9 and 10 are available in HEPData [46].

The polarization of τ^- leptons produced in Z bosons decays is a direct consequence of the structure of the weak interaction, namely the mixing of the B^0 and the W^0 fields, which is parametrized by the effective mixing angle, $\sin^2\theta_W^{\text{eff}}$. In the analysis it is not possible to distinguish between $Z \to \tau^+\tau^-$ and $\gamma \to \tau^+\tau^-$, because they produce exactly the same final state. The $\gamma \to \tau^+\tau^-$ process results in unpolarized τ^- leptons. Because the relative fraction

JHEP01(2024)101

of $\mathrm{Z}/\gamma \to \tau^+\tau^-$ events changes as a function of the quark-antiquark invariant mass $\sqrt{\hat{s}}$, the polarization has to be considered as a function of this mass, the effective mixing angle, and the quark type, specifying whether the Z has been produced via a pair of up- or down-type quarks, see eq. (9.2). This average has been accounted for in our procedure described in section 9 to correct the measured polarization to the Z pole. This result can be directly used in the relation of eq. (1.5) to obtain a value for the effective electroweak mixing angle:

$$\sin^2\theta_{\mathrm{W}}^{\mathrm{eff}} = 0.2319 \pm 0.0008\,(\mathrm{stat}) \pm 0.0018\,(\mathrm{syst}) = 0.2319 \pm 0.0019. \tag{10.3}$$

Our result is in good agreement with the most precise value of the effective weak mixing angle measured in $\mathrm{Z} \to \ell^+\ell^-$ decays obtained by the combination of the LEP and SLD results $\sin^2\theta_{\mathrm{W}}^{\mathrm{eff}} = 0.2315 \pm 0.0002$ [43].

11 Summary

The CMS detector was used to measure the polarization of τ^- leptons in the decay of Z bosons produced in proton-proton collisions at the LHC at $\sqrt{s} = 13\,\mathrm{TeV}$ in a data sample corresponding to an integrated luminosity of $36.3\,\mathrm{fb}^{-1}$. Eleven different combinations of decay modes of the τ leptons were used to study the polarization.

The measured τ^- lepton polarization, $\mathcal{P}_\tau(\mathrm{Z}) = -0.144 \pm 0.006\,(\mathrm{stat}) \pm 0.014\,(\mathrm{syst}) = -0.144 \pm 0.015$, is in good agreement with the SLD, LEP and ATLAS results. It is also compatible with the world average value of the lepton asymmetry parameter A_ℓ [45]. This result is at present the most precise measurement at hadron colliders and reaches a similar precision to the SLD experiment.

The measured polarization constrains the effective couplings of τ^- leptons to the Z boson and determines the effective weak mixing angle to be $\sin^2\theta_{\mathrm{W}}^{\mathrm{eff}} = 0.2319 \pm 0.0019$. This result has a precision of 0.8% and is independent of the production process of the Z boson.

Acknowledgments

We congratulate our colleagues in the CERN accelerator departments for the excellent performance of the LHC and thank the technical and administrative staffs at CERN and at other CMS institutes for their contributions to the success of the CMS effort. In addition, we gratefully acknowledge the computing centers and personnel of the Worldwide LHC Computing Grid and other centers for delivering so effectively the computing infrastructure essential to our analyses. Finally, we acknowledge the enduring support for the construction and operation of the LHC, the CMS detector, and the supporting computing infrastructure provided by the following funding agencies: SC (Armenia), BMBWF and FWF (Austria); FNRS and FWO (Belgium); CNPq, CAPES, FAPERJ, FAPERGS, and FAPESP (Brazil); MES and BNSF (Bulgaria); CERN; CAS, MoST, and NSFC (China); MINCIENCIAS (Colombia); MSES and CSF (Croatia); RIF (Cyprus); SENESCYT (Ecuador); MoER, ERC PUT and ERDF (Estonia); Academy of Finland, MEC, and HIP (Finland); CEA and CNRS/IN2P3 (France); SRNSF (Georgia); BMBF, DFG, and HGF (Germany); GSRI (Greece); NKFIH (Hungary); DAE and DST (India); IPM (Iran); SFI (Ireland); INFN (Italy); MSIP and NRF

JHEP01(2024)101

(Republic of Korea); MES (Latvia); LAS (Lithuania); MOE and UM (Malaysia); BUAP, CINVESTAV, CONACYT, LNS, SEP, and UASLP-FAI (Mexico); MOS (Montenegro); MBIE (New Zealand); PAEC (Pakistan); MES and NSC (Poland); FCT (Portugal); MESTD (Serbia); MCIN/AEI and PCTI (Spain); MOSTR (Sri Lanka); Swiss Funding Agencies (Switzerland); MST (Taipei); MHESI and NSTDA (Thailand); TUBITAK and TENMAK (Turkey); NASU (Ukraine); STFC (United Kingdom); DOE and NSF (U.S.A.).

Individuals have received support from the Marie-Curie program and the European Research Council and Horizon 2020 Grant, contract Nos. 675440, 724704, 752730, 758316, 765710, 824093, and COST Action CA16108 (European Union); the Leventis Foundation; the Alfred P. Sloan Foundation; the Alexander von Humboldt Foundation; the Science Committee, project no. 22rl-037 (Armenia); the Belgian Federal Science Policy Office; the Fonds pour la Formation à la Recherche dans l'Industrie et dans l'Agriculture (FRIA-Belgium); the Agentschap voor Innovatie door Wetenschap en Technologie (IWT-Belgium); the F.R.S.-FNRS and FWO (Belgium) under the "Excellence of Science —EOS" —be.h project n. 30820817; the Beijing Municipal Science & Technology Commission, No. Z191100007219010 and Fundamental Research Funds for the Central Universities (China); the Ministry of Education, Youth and Sports (MEYS) of the Czech Republic; the Shota Rustaveli National Science Foundation, grant FR-22-985 (Georgia); the Deutsche Forschungsgemeinschaft (DFG), under Germany's Excellence Strategy —EXC 2121 "Quantum Universe" —390833306, and under project number 400140256 —GRK2497; the Hellenic Foundation for Research and Innovation (HFRI), Project Number 2288 (Greece); the Hungarian Academy of Sciences, the New National Excellence Program —ÚNKP, the NKFIH research grants K 124845, K 124850, K 128713, K 128786, K 129058, K 131991, K 133046, K 138136, K 143460, K 143477, 2020-2.2.1-ED-2021-00181, and TKP2021-NKTA-64 (Hungary); the Council of Science and Industrial Research, India; the Latvian Council of Science; the Ministry of Education and Science, project no. 2022/WK/14, and the National Science Center, contracts Opus 2021/41/B/ST2/01369 and 2021/43/B/ST2/01552 (Poland); the Fundação para a Ciência e a Tecnologia, grant CEECIND/01334/2018 (Portugal); the National Priorities Research Program by Qatar National Research Fund; MCIN/AEI/10.13039/501100011033, ERDF "a way of making Europe", and the Programa Estatal de Fomento de la Investigación Científica y Técnica de Excelencia María de Maeztu, grant MDM-2017-0765 and Programa Severo Ochoa del Principado de Asturias (Spain); the Chulalongkorn Academic into Its 2nd Century Project Advancement Project, and the National Science, Research and Innovation Fund via the Program Management Unit for Human Resources & Institutional Development, Research and Innovation, grant B05F650021 (Thailand); the Kavli Foundation; the Nvidia Corporation; the SuperMicro Corporation; the Welch Foundation, contract C-1845; and the Weston Havens Foundation (U.S.A.).

JHEP01(2024)101

References

[1] J.A. Fuster et al., *The tau polarization measurement at LEP*, CERN-EP-89-129, CERN, Geneva, Switzerland (1989) [DOI:10.5170/CERN-1989-008-V-1.235].

[2] ALEPH collaboration, *Measurement of the tau polarization at LEP*, *Eur. Phys. J. C* **20** (2001) 401 [hep-ex/0104038] [INSPIRE].

[3] DELPHI collaboration, *A precise measurement of the tau polarization at LEP-1*, *Eur. Phys. J. C* **14** (2000) 585 [INSPIRE].

[4] L3 collaboration, *Measurement of tau polarization at LEP*, *Phys. Lett. B* **429** (1998) 387 [INSPIRE].

[5] OPAL collaboration, *Precision neutral current asymmetry parameter measurements from the tau polarization at LEP*, *Eur. Phys. J. C* **21** (2001) 1 [hep-ex/0103045] [INSPIRE].

[6] SLD collaboration, *An improved direct measurement of leptonic coupling asymmetries with polarized Z bosons*, *Phys. Rev. Lett.* **86** (2001) 1162 [hep-ex/0010015] [INSPIRE].

[7] ATLAS collaboration, *Measurement of τ polarisation in $Z/\gamma^* \to \tau\tau$ decays in proton-proton collisions at $\sqrt{s} = 8$ TeV with the ATLAS detector*, *Eur. Phys. J. C* **78** (2018) 163 [arXiv:1709.03490] [INSPIRE].

[8] CMS collaboration, *The CMS experiment at the CERN LHC*, 2008 *JINST* **3** S08004 [INSPIRE].

[9] CMS collaboration, *Performance of the CMS level-1 trigger in proton-proton collisions at $\sqrt{s} = 13$ TeV*, 2020 *JINST* **15** P10017 [arXiv:2006.10165] [INSPIRE].

[10] CMS collaboration, *The CMS trigger system*, 2017 *JINST* **12** P01020 [arXiv:1609.02366] [INSPIRE].

[11] CMS collaboration, *Precision luminosity measurement in proton-proton collisions at $\sqrt{s} = 13$ TeV in* 2015 *and* 2016 *at CMS*, *Eur. Phys. J. C* **81** (2021) 800 [arXiv:2104.01927] [INSPIRE].

[12] J. Alwall et al., *The automated computation of tree-level and next-to-leading order differential cross sections, and their matching to parton shower simulations*, *JHEP* **07** (2014) 079 [arXiv:1405.0301] [INSPIRE].

[13] T. Sjöstrand et al., *An introduction to PYTHIA* 8.2, *Comput. Phys. Commun.* **191** (2015) 159 [arXiv:1410.3012] [INSPIRE].

[14] CMS collaboration, *Event generator tunes obtained from underlying event and multiparton scattering measurements*, *Eur. Phys. J. C* **76** (2016) 155 [arXiv:1512.00815] [INSPIRE].

[15] S. Jadach, Z. Was, R. Decker and J.H. Kühn, *The tau decay library TAUOLA: version* 2.4, *Comput. Phys. Commun.* **76** (1993) 361 [INSPIRE].

[16] N. Davidson et al., *Universal interface of TAUOLA technical and physics documentation*, *Comput. Phys. Commun.* **183** (2012) 821 [arXiv:1002.0543] [INSPIRE].

[17] NNPDF collaboration, *Parton distributions for the LHC run II*, *JHEP* **04** (2015) 040 [arXiv:1410.8849] [INSPIRE].

[18] GEANT4 collaboration, *GEANT4 — a simulation toolkit*, *Nucl. Instrum. Meth. A* **506** (2003) 250 [INSPIRE].

[19] CMS collaboration, *Observation of the Higgs boson decay to a pair of τ leptons with the CMS detector*, *Phys. Lett. B* **779** (2018) 283 [arXiv:1708.00373] [INSPIRE].

JHEP01(2024)101

[20] E. Re, *Single-top Wt-channel production matched with parton showers using the POWHEG method*, *Eur. Phys. J. C* **71** (2011) 1547 [arXiv:1009.2450] [INSPIRE].

[21] S. Alioli, P. Nason, C. Oleari and E. Re, *NLO single-top production matched with shower in POWHEG: s- and t-channel contributions*, *JHEP* **09** (2009) 111 [*Erratum ibid.* **02** (2010) 011] [arXiv:0907.4076] [INSPIRE].

[22] S. Frixione, P. Nason and G. Ridolfi, *A positive-weight next-to-leading-order Monte Carlo for heavy flavour hadroproduction*, *JHEP* **09** (2007) 126 [arXiv:0707.3088] [INSPIRE].

[23] CMS collaboration, *Investigations of the impact of the parton shower tuning in Pythia 8 in the modelling of $t\bar{t}$ at $\sqrt{s} = 8$ and 13 TeV*, CMS-PAS-TOP-16-021, CERN, Geneva (2016).

[24] CMS collaboration, *Pileup mitigation at CMS in 13 TeV data*, 2020 *JINST* **15** P09018 [arXiv:2003.00503] [INSPIRE].

[25] CMS collaboration, *Particle-flow reconstruction and global event description with the CMS detector*, 2017 *JINST* **12** P10003 [arXiv:1706.04965] [INSPIRE].

[26] M. Cacciari, G.P. Salam and G. Soyez, *The anti-k_t jet clustering algorithm*, *JHEP* **04** (2008) 063 [arXiv:0802.1189] [INSPIRE].

[27] M. Cacciari, G.P. Salam and G. Soyez, *FastJet user manual*, *Eur. Phys. J. C* **72** (2012) 1896 [arXiv:1111.6097] [INSPIRE].

[28] CMS collaboration, *Jet energy scale and resolution in the CMS experiment in pp collisions at 8 TeV*, 2017 *JINST* **12** P02014 [arXiv:1607.03663] [INSPIRE].

[29] CMS collaboration, *Electron and photon reconstruction and identification with the CMS experiment at the CERN LHC*, 2021 *JINST* **16** P05014 [arXiv:2012.06888] [INSPIRE].

[30] CMS collaboration, *Performance of CMS muon reconstruction in pp collision events at $\sqrt{s} = 7$ TeV*, 2012 *JINST* **7** P10002 [arXiv:1206.4071] [INSPIRE].

[31] CMS collaboration, *Performance of missing transverse momentum reconstruction in proton-proton collisions at $\sqrt{s} = 13$ TeV using the CMS detector*, 2019 *JINST* **14** P07004 [arXiv:1903.06078] [INSPIRE].

[32] D. Bertolini, P. Harris, M. Low and N. Tran, *Pileup per particle identification*, *JHEP* **10** (2014) 059 [arXiv:1407.6013] [INSPIRE].

[33] CMS collaboration, *Measurement of inclusive W and Z boson production cross sections in pp collisions at $\sqrt{s} = 8$ TeV*, *Phys. Rev. Lett.* **112** (2014) 191802 [arXiv:1402.0923] [INSPIRE].

[34] CMS collaboration, *Performance of reconstruction and identification of τ leptons decaying to hadrons and ν_τ in pp collisions at $\sqrt{s} = 13$ TeV*, 2018 *JINST* **13** P10005 [arXiv:1809.02816] [INSPIRE].

[35] CMS collaboration, *Analysis of the CP structure of the Yukawa coupling between the Higgs boson and τ leptons in proton-proton collisions at $\sqrt{s} = 13$ TeV*, *JHEP* **06** (2022) 012 [arXiv:2110.04836] [INSPIRE].

[36] CMS collaboration, *Identification of hadronic tau lepton decays using a deep neural network*, 2022 *JINST* **17** P07023 [arXiv:2201.08458] [INSPIRE].

[37] Y.-S. Tsai, *Decay correlations of heavy leptons in $e^+e^- \to \ell^+\ell^-$*, *Phys. Rev. D* **4** (1971) 2821 [*Erratum ibid.* **13** (1976) 771] [INSPIRE].

[38] V. Cherepanov and W. Lohmann, *Methods for a measurement of τ polarization asymmetry in the decay $Z \to \tau\tau$ at LHC and determination of the effective weak mixing angle*, arXiv:1805.10552 [INSPIRE].

JHEP01(2024)101

[39] M. Davier, L. Duflot, F. Le Diberder and A. Rouge, *The optimal method for the measurement of tau polarization*, *Phys. Lett. B* **306** (1993) 411 [INSPIRE].

[40] CLEO collaboration, *Hadronic structure in the decay $\tau^- \to \pi^-\pi^0\pi^0\nu_\tau$ and the sign of the ν_τ helicity*, *Phys. Rev. D* **61** (2000) 012002 [hep-ex/9902022] [INSPIRE].

[41] L. Bianchini et al., *Reconstruction of the Higgs mass in events with Higgs bosons decaying into a pair of τ leptons using matrix element techniques*, *Nucl. Instrum. Meth. A* **862** (2017) 54 [arXiv:1603.05910] [INSPIRE].

[42] R. Alemany et al., *Tau polarization at the Z peak from the acollinearity between both tau decay products*, *Nucl. Phys. B* **379** (1992) 3 [INSPIRE].

[43] ALEPH et al. collaborations, *Precision electroweak measurements on the Z resonance*, *Phys. Rept.* **427** (2006) 257 [hep-ex/0509008] [INSPIRE].

[44] A. Akhundov, A. Arbuzov, S. Riemann and T. Riemann, *The ZFITTER project*, *Phys. Part. Nucl.* **45** (2014) 529 [arXiv:1302.1395] [INSPIRE].

[45] Particle Data Group collaboration, *Review of particle physics*, *PTEP* **2022** (2022) 083C01 [INSPIRE].

[46] *HEPData record for this analysis*, CMS-SMP-18-010 (2023) [DOI:10.17182/HEPDATA.144221].

JHEP01(2024)101

The CMS collaboration

Yerevan Physics Institute, Yerevan, Armenia

A. Hayrapetyan, A. Tumasyan[1]

Institut für Hochenergiephysik, Vienna, Austria

W. Adam, J.W. Andrejkovic, T. Bergauer, S. Chatterjee, K. Damanakis, M. Dragicevic, A. Escalante Del Valle, P.S. Hussain, M. Jeitler[2], N. Krammer, D. Liko, I. Mikulec, J. Schieck[2], R. Schöfbeck, D. Schwarz, M. Sonawane, S. Templ, W. Waltenberger, C.-E. Wulz[2]

Universiteit Antwerpen, Antwerpen, Belgium

M.R. Darwish[3], T. Janssen, P. Van Mechelen

Vrije Universiteit Brussel, Brussel, Belgium

E.S. Bols, J. D'Hondt, S. Dansana, A. De Moor, M. Delcourt, H. El Faham, S. Lowette, I. Makarenko, D. Müller, A.R. Sahasransu, S. Tavernier, M. Tytgat[4], S. Van Putte, D. Vannerom

Université Libre de Bruxelles, Bruxelles, Belgium

B. Clerbaux, G. De Lentdecker, L. Favart, D. Hohov, J. Jaramillo, A. Khalilzadeh, K. Lee, M. Mahdavikhorrami, A. Malara, S. Paredes, L. Pétré, N. Postiau, L. Thomas, M. Vanden Bemden, C. Vander Velde, P. Vanlaer

Ghent University, Ghent, Belgium

M. De Coen, D. Dobur, Y. Hong, J. Knolle, L. Lambrecht, G. Mestdach, C. Rendón, A. Samalan, K. Skovpen, N. Van Den Bossche, L. Wezenbeek

Université Catholique de Louvain, Louvain-la-Neuve, Belgium

A. Benecke, G. Bruno, C. Caputo, C. Delaere, I.S. Donertas, A. Giammanco, K. Jaffel, Sa. Jain, V. Lemaitre, J. Lidrych, P. Mastrapasqua, K. Mondal, T.T. Tran, S. Wertz

Centro Brasileiro de Pesquisas Fisicas, Rio de Janeiro, Brazil

G.A. Alves, E. Coelho, C. Hensel, T. Menezes De Oliveira, A. Moraes, P. Rebello Teles, M. Soeiro

Universidade do Estado do Rio de Janeiro, Rio de Janeiro, Brazil

W.L. Aldá Júnior, M. Alves Gallo Pereira, M. Barroso Ferreira Filho, H. Brandao Malbouisson, W. Carvalho, J. Chinellato[5], E.M. Da Costa, G.G. Da Silveira[6], D. De Jesus Damiao, S. Fonseca De Souza, J. Martins[7], C. Mora Herrera, K. Mota Amarilo, L. Mundim, H. Nogima, A. Santoro, S.M. Silva Do Amaral, A. Sznajder, M. Thiel, A. Vilela Pereira

Universidade Estadual Paulista, Universidade Federal do ABC, São Paulo, Brazil

C.A. Bernardes[6], L. Calligaris, T.R. Fernandez Perez Tomei, E.M. Gregores, P.G. Mercadante, S.F. Novaes, B. Orzari, Sandra S. Padula

JHEP01(2024)101

Institute for Nuclear Research and Nuclear Energy, Bulgarian Academy of Sciences, Sofia, Bulgaria

A. Aleksandrov, G. Antchev, R. Hadjiiska, P. Iaydjiev, M. Misheva, M. Shopova, G. Sultanov

University of Sofia, Sofia, Bulgaria

A. Dimitrov, T. Ivanov, L. Litov, B. Pavlov, P. Petkov, A. Petrov, E. Shumka

Instituto De Alta Investigación, Universidad de Tarapacá, Casilla 7 D, Arica, Chile

S. Keshri, S. Thakur

Beihang University, Beijing, China

T. Cheng, Q. Guo, T. Javaid, M. Mittal, L. Yuan

Department of Physics, Tsinghua University, Beijing, China

G. Bauer[8], Z. Hu, K. Yi[8,9]

Institute of High Energy Physics, Beijing, China

G.M. Chen[10], H.S. Chen[10], M. Chen[10], F. Iemmi, C.H. Jiang, A. Kapoor, H. Liao, Z.-A. Liu[11], F. Monti, R. Sharma, J.N. Song[11], J. Tao, C. Wang[10], J. Wang, Z. Wang, H. Zhang

State Key Laboratory of Nuclear Physics and Technology, Peking University, Beijing, China

A. Agapitos, Y. Ban, A. Levin, C. Li, Q. Li, X. Lyu, Y. Mao, S.J. Qian, X. Sun, D. Wang, H. Yang, C. Zhou

Sun Yat-Sen University, Guangzhou, China

Z. You

University of Science and Technology of China, Hefei, China

N. Lu

Institute of Modern Physics and Key Laboratory of Nuclear Physics and Ion-beam Application (MOE) — Fudan University, Shanghai, China

X. Gao[12], D. Leggat, H. Okawa, Y. Zhang

Zhejiang University, Hangzhou, Zhejiang, China

Z. Lin, C. Lu, M. Xiao

Universidad de Los Andes, Bogota, Colombia

C. Avila, D.A. Barbosa Trujillo, A. Cabrera, C. Florez, J. Fraga, J.A. Reyes Vega

Universidad de Antioquia, Medellin, Colombia

J. Mejia Guisao, F. Ramirez, M. Rodriguez, J.D. Ruiz Alvarez

JHEP01(2024)101

University of Split, Faculty of Electrical Engineering, Mechanical Engineering and Naval Architecture, Split, Croatia
D. Giljanovic, N. Godinovic, D. Lelas, A. Sculac

University of Split, Faculty of Science, Split, Croatia
M. Kovac, T. Sculac

Institute Rudjer Boskovic, Zagreb, Croatia
P. Bargassa, V. Brigljevic, B.K. Chitroda, D. Ferencek, S. Mishra, A. Starodumov[13], T. Susa

University of Cyprus, Nicosia, Cyprus
A. Attikis, K. Christoforou, S. Konstantinou, J. Mousa, C. Nicolaou, F. Ptochos, P.A. Razis, H. Rykaczewski, H. Saka, A. Stepennov

Charles University, Prague, Czech Republic
M. Finger, M. Finger Jr., A. Kveton

Escuela Politecnica Nacional, Quito, Ecuador
E. Ayala

Universidad San Francisco de Quito, Quito, Ecuador
E. Carrera Jarrin

Academy of Scientific Research and Technology of the Arab Republic of Egypt, Egyptian Network of High Energy Physics, Cairo, Egypt
Y. Assran[14,15], S. Elgammal[15]

Center for High Energy Physics (CHEP-FU), Fayoum University, El-Fayoum, Egypt
A. Lotfy, M.A. Mahmoud

National Institute of Chemical Physics and Biophysics, Tallinn, Estonia
R.K. Dewanjee[16], K. Ehataht, M. Kadastik, T. Lange, S. Nandan, C. Nielsen, J. Pata, M. Raidal, L. Tani, C. Veelken

Department of Physics, University of Helsinki, Helsinki, Finland
H. Kirschenmann, K. Osterberg, M. Voutilainen

Helsinki Institute of Physics, Helsinki, Finland
S. Bharthuar, E. Brücken, F. Garcia, J. Havukainen, K.T.S. Kallonen, M.S. Kim, R. Kinnunen, T. Lampén, K. Lassila-Perini, S. Lehti, T. Lindén, M. Lotti, L. Martikainen, M. Myllymäki, M.m. Rantanen, H. Siikonen, E. Tuominen, J. Tuominiemi

Lappeenranta-Lahti University of Technology, Lappeenranta, Finland
P. Luukka, H. Petrow, T. Tuuva[†]

JHEP01(2024)101

IRFU, CEA, Université Paris-Saclay, Gif-sur-Yvette, France

M. Besancon, F. Couderc, M. Dejardin, D. Denegri, J.L. Faure, F. Ferri, S. Ganjour, P. Gras, G. Hamel de Monchenault, V. Lohezic, J. Malcles, J. Rander, A. Rosowsky, M.Ö. Sahin, A. Savoy-Navarro[17], P. Simkina, M. Titov

Laboratoire Leprince-Ringuet, CNRS/IN2P3, Ecole Polytechnique, Institut Polytechnique de Paris, Palaiseau, France

C. Baldenegro Barrera, F. Beaudette, A. Buchot Perraguin, P. Busson, A. Cappati, C. Charlot, F. Damas, O. Davignon, A. De Wit, G. Falmagne, B.A. Fontana Santos Alves, S. Ghosh, A. Gilbert, R. Granier de Cassagnac, A. Hakimi, B. Harikrishnan, L. Kalipoliti, G. Liu, J. Motta, M. Nguyen, C. Ochando, L. Portales, R. Salerno, U. Sarkar, J.B. Sauvan, Y. Sirois, A. Tarabini, E. Vernazza, A. Zabi, A. Zghiche

Université de Strasbourg, CNRS, IPHC UMR 7178, Strasbourg, France

J.-L. Agram[18], J. Andrea, D. Apparu, D. Bloch, J.-M. Brom, E.C. Chabert, C. Collard, S. Falke, U. Goerlach, C. Grimault, R. Haeberle, A.-C. Le Bihan, M.A. Sessini, P. Van Hove

Institut de Physique des 2 Infinis de Lyon (IP2I), Villeurbanne, France

S. Beauceron, B. Blancon, G. Boudoul, N. Chanon, J. Choi, D. Contardo, P. Depasse, C. Dozen[19], H. El Mamouni, J. Fay, S. Gascon, M. Gouzevitch, C. Greenberg, G. Grenier, B. Ille, I.B. Laktineh, M. Lethuillier, L. Mirabito, S. Perries, M. Vander Donckt, P. Verdier, J. Xiao

Georgian Technical University, Tbilisi, Georgia

D. Chokheli, I. Lomidze, Z. Tsamalaidze[13]

RWTH Aachen University, I. Physikalisches Institut, Aachen, Germany

V. Botta, L. Feld, K. Klein, M. Lipinski, D. Meuser, A. Pauls, N. Röwert, M. Teroerde

RWTH Aachen University, III. Physikalisches Institut A, Aachen, Germany

S. Diekmann, A. Dodonova, N. Eich, D. Eliseev, F. Engelke, M. Erdmann, P. Fackeldey, B. Fischer, T. Hebbeker, K. Hoepfner, F. Ivone, A. Jung, M.y. Lee, L. Mastrolorenzo, M. Merschmeyer, A. Meyer, S. Mukherjee, D. Noll, A. Novak, F. Nowotny, A. Pozdnyakov, Y. Rath, W. Redjeb, F. Rehm, H. Reithler, V. Sarkisovi, A. Schmidt, S.C. Schuler, A. Sharma, A. Stein, F. Torres Da Silva De Araujo[20], L. Vigilante, S. Wiedenbeck, S. Zaleski

RWTH Aachen University, III. Physikalisches Institut B, Aachen, Germany

C. Dziwok, G. Flügge, W. Haj Ahmad[21], T. Kress, A. Nowack, O. Pooth, A. Stahl, T. Ziemons, A. Zotz

Deutsches Elektronen-Synchrotron, Hamburg, Germany

H. Aarup Petersen, M. Aldaya Martin, J. Alimena, S. Amoroso, Y. An, S. Baxter, M. Bayatmakou, H. Becerril Gonzalez, O. Behnke, A. Belvedere, S. Bhattacharya,

JHEP01(2024)101

F. Blekman[22], K. Borras[23], D. Brunner, A. Campbell, A. Cardini, C. Cheng, F. Colombina, S. Consuegra Rodríguez, G. Correia Silva, M. De Silva, G. Eckerlin, D. Eckstein, L.I. Estevez Banos, O. Filatov, E. Gallo[22], A. Geiser, A. Giraldi, G. Greau, V. Guglielmi, M. Guthoff, A. Hinzmann, A. Jafari[24], L. Jeppe, N.Z. Jomhari, B. Kaech, M. Kasemann, H. Kaveh, C. Kleinwort, R. Kogler, M. Komm, D. Krücker, W. Lange, D. Leyva Pernia, K. Lipka[25], W. Lohmann[26], R. Mankel, I.-A. Melzer-Pellmann, M. Mendizabal Morentin, J. Metwally, A.B. Meyer, G. Milella, A. Mussgiller, A. Nürnberg, Y. Otarid, D. Pérez Adán, E. Ranken, A. Raspereza, B. Ribeiro Lopes, J. Rübenach, A. Saggio, M. Scham[27,23], V. Scheurer, S. Schnake[23], P. Schütze, C. Schwanenberger[22], M. Shchedrolosiev, R.E. Sosa Ricardo, L.P. Sreelatha Pramod, D. Stafford, F. Vazzoler, A. Ventura Barroso, R. Walsh, Q. Wang, Y. Wen, K. Wichmann, L. Wiens[23], C. Wissing, S. Wuchterl, Y. Yang, A. Zimermmane Castro Santos

University of Hamburg, Hamburg, Germany

A. Albrecht, S. Albrecht, M. Antonello, S. Bein, L. Benato, M. Bonanomi, P. Connor, M. Eich, K. El Morabit, Y. Fischer, A. Fröhlich, C. Garbers, E. Garutti, A. Grohsjean, M. Hajheidari, J. Haller, H.R. Jabusch, G. Kasieczka, P. Keicher, R. Klanner, W. Korcari, T. Kramer, V. Kutzner, F. Labe, J. Lange, A. Lobanov, C. Matthies, A. Mehta, L. Moureaux, M. Mrowietz, A. Nigamova, Y. Nissan, A. Paasch, K.J. Pena Rodriguez, T. Quadfasel, B. Raciti, M. Rieger, D. Savoiu, J. Schindler, P. Schleper, M. Schröder, J. Schwandt, M. Sommerhalder, H. Stadie, G. Steinbrück, A. Tews, M. Wolf

Karlsruher Institut fuer Technologie, Karlsruhe, Germany

S. Brommer, M. Burkart, E. Butz, T. Chwalek, A. Dierlamm, A. Droll, N. Faltermann, M. Giffels, A. Gottmann, F. Hartmann[28], M. Horzela, U. Husemann, M. Klute, R. Koppenhöfer, M. Link, A. Lintuluoto, S. Maier, S. Mitra, M. Mormile, Th. Müller, M. Neukum, M. Oh, G. Quast, K. Rabbertz, I. Shvetsov, H.J. Simonis, N. Trevisani, R. Ulrich, J. van der Linden, R.F. Von Cube, M. Wassmer, S. Wieland, F. Wittig, R. Wolf, S. Wunsch, X. Zuo

Institute of Nuclear and Particle Physics (INPP), NCSR Demokritos, Aghia Paraskevi, Greece

G. Anagnostou, P. Assiouras, G. Daskalakis, A. Kyriakis, A. Papadopoulos[28], A. Stakia

National and Kapodistrian University of Athens, Athens, Greece

D. Karasavvas, P. Kontaxakis, G. Melachroinos, A. Panagiotou, I. Papavergou, I. Paraskevas, N. Saoulidou, K. Theofilatos, E. Tziaferi, K. Vellidis, I. Zisopoulos

National Technical University of Athens, Athens, Greece

G. Bakas, T. Chatzistavrou, G. Karapostoli, K. Kousouris, I. Papakrivopoulos, E. Siamarkou, G. Tsipolitis, A. Zacharopoulou

University of Ioánnina, Ioánnina, Greece

K. Adamidis, I. Bestintzanos, I. Evangelou, C. Foudas, P. Gianneios, C. Kamtsikis, P. Katsoulis, P. Kokkas, P.G. Kosmoglou Kioseoglou, N. Manthos, I. Papadopoulos, J. Strologas

JHEP01(2024)101

MTA-ELTE Lendület CMS Particle and Nuclear Physics Group, Eötvös Loránd University, Budapest, Hungary

M. Csanád, K. Farkas, M.M.A. Gadallah[29], Á. Kadlecsik, P. Major, K. Mandal, G. Pásztor, A.J. Rádl[30], G.I. Veres

Wigner Research Centre for Physics, Budapest, Hungary

M. Bartók[31], C. Hajdu, D. Horvath[32,33], F. Sikler, V. Veszpremi

Faculty of Informatics, University of Debrecen, Debrecen, Hungary

P. Raics, B. Ujvari[34], G. Zilizi

Institute of Nuclear Research ATOMKI, Debrecen, Hungary

G. Bencze, S. Czellar, J. Karancsi[31], J. Molnar, Z. Szillasi

Karoly Robert Campus, MATE Institute of Technology, Gyongyos, Hungary

T. Csorgo[30], F. Nemes[30], T. Novak

Panjab University, Chandigarh, India

J. Babbar, S. Bansal, S.B. Beri, V. Bhatnagar, G. Chaudhary, S. Chauhan, N. Dhingra[35], R. Gupta, A. Kaur, A. Kaur, H. Kaur, M. Kaur, S. Kumar, P. Kumari, M. Meena, K. Sandeep, T. Sheokand, J.B. Singh[36], A. Singla

University of Delhi, Delhi, India

A. Ahmed, A. Bhardwaj, A. Chhetri, B.C. Choudhary, A. Kumar, M. Naimuddin, K. Ranjan, S. Saumya

Saha Institute of Nuclear Physics, HBNI, Kolkata, India

S. Baradia, S. Barman[37], S. Bhattacharya, D. Bhowmik, S. Dutta, S. Dutta, B. Gomber[38], P. Palit, G. Saha, B. Sahu[38], S. Sarkar

Indian Institute of Technology Madras, Madras, India

M.M. Ameen, P.K. Behera, S.C. Behera, S. Chatterjee, P. Jana, P. Kalbhor, J.R. Komaragiri[39], D. Kumar[39], L. Panwar[39], R. Pradhan, P.R. Pujahari, N.R. Saha, A. Sharma, A.K. Sikdar, S. Verma

Tata Institute of Fundamental Research-A, Mumbai, India

T. Aziz, I. Das, S. Dugad, M. Kumar, G.B. Mohanty, P. Suryadevara

Tata Institute of Fundamental Research-B, Mumbai, India

A. Bala, S. Banerjee, R.M. Chatterjee, M. Guchait, S. Karmakar, S. Kumar, G. Majumder, K. Mazumdar, S. Mukherjee, A. Thachayath

National Institute of Science Education and Research, An OCC of Homi Bhabha National Institute, Bhubaneswar, Odisha, India

S. Bahinipati[40], A.K. Das, C. Kar, D. Maity[41], P. Mal, T. Mishra, V.K. Muraleedharan Nair Bindhu[41], K. Naskar[41], A. Nayak[41], P. Sadangi, P. Saha, S.K. Swain, S. Varghese[41], D. Vats[41]

JHEP01(2024)101

Indian Institute of Science Education and Research (IISER), Pune, India
A. Alpana, S. Dube, B. Kansal, A. Laha, A. Rastogi, S. Sharma

Isfahan University of Technology, Isfahan, Iran
H. Bakhshiansohi[42], E. Khazaie[43], M. Zeinali[44]

Institute for Research in Fundamental Sciences (IPM), Tehran, Iran
S. Chenarani[45], S.M. Etesami, M. Khakzad, M. Mohammadi Najafabadi

University College Dublin, Dublin, Ireland
M. Grunewald

INFN Sezione di Bari[a], Università di Bari[b], Politecnico di Bari[c], Bari, Italy
M. Abbrescia[a,b], R. Aly[a,c,46], A. Colaleo[a,b], D. Creanza[a,c], B. D' Anzi[a,b], N. De Filippis[a,c], M. De Palma[a,b], A. Di Florio[a,c], W. Elmetenawee[a,b,46], L. Fiore[a], G. Iaselli[a,c], G. Maggi[a,c], M. Maggi[a], I. Margjeka[a,b], V. Mastrapasqua[a,b], S. My[a,b], S. Nuzzo[a,b], A. Pellecchia[a,b], A. Pompili[a,b], G. Pugliese[a,c], R. Radogna[a], G. Ramirez-Sanchez[a,c], D. Ramos[a], A. Ranieri[a], L. Silvestris[a], F.M. Simone[a,b], Ü. Sözbilir[a], A. Stamerra[a], R. Venditti[a], P. Verwilligen[a], A. Zaza[a,b]

INFN Sezione di Bologna[a], Università di Bologna[b], Bologna, Italy
G. Abbiendi[a], C. Battilana[a,b], D. Bonacorsi[a,b], L. Borgonovi[a], R. Campanini[a,b], P. Capiluppi[a,b], F.R. Cavallo[a], M. Cuffiani[a,b], G.M. Dallavalle[a], T. Diotalevi[a,b], F. Fabbri[a], A. Fanfani[a,b], D. Fasanella[a,b], P. Giacomelli[a], L. Giommi[a,b], C. Grandi[a], L. Guiducci[a,b], S. Lo Meo[a,47], L. Lunerti[a,b], S. Marcellini[a], G. Masetti[a], F.L. Navarria[a,b], A. Perrotta[a], F. Primavera[a,b], A.M. Rossi[a,b], T. Rovelli[a,b], G.P. Siroli[a,b]

INFN Sezione di Catania[a], Università di Catania[b], Catania, Italy
S. Costa[a,b,48], A. Di Mattia[a], R. Potenza[a,b], A. Tricomi[a,b,48], C. Tuve[a,b]

INFN Sezione di Firenze[a], Università di Firenze[b], Firenze, Italy
G. Barbagli[a], G. Bardelli[a,b], B. Camaiani[a,b], A. Cassese[a], R. Ceccarelli[a], V. Ciulli[a,b], C. Civinini[a], R. D'Alessandro[a,b], E. Focardi[a,b], G. Latino[a,b], P. Lenzi[a,b], M. Lizzo[a,b], M. Meschini[a], S. Paoletti[a], A. Papanastassiou[a,b], G. Sguazzoni[a], L. Viliani[a]

INFN Laboratori Nazionali di Frascati, Frascati, Italy
L. Benussi, S. Bianco, S. Meola[49], D. Piccolo

INFN Sezione di Genova[a], Università di Genova[b], Genova, Italy
P. Chatagnon[a], F. Ferro[a], E. Robutti[a], S. Tosi[a,b]

INFN Sezione di Milano-Bicocca[a], Università di Milano-Bicocca[b], Milano, Italy
A. Benaglia[a], G. Boldrini[a], F. Brivio[a], F. Cetorelli[a], F. De Guio[a,b], M.E. Dinardo[a,b], P. Dini[a], S. Gennai[a], A. Ghezzi[a,b], P. Govoni[a,b], L. Guzzi[a], M.T. Lucchini[a,b], M. Malberti[a], S. Malvezzi[a], A. Massironi[a], D. Menasce[a], L. Moroni[a], M. Paganoni[a,b], D. Pedrini[a], B.S. Pinolini[a], S. Ragazzi[a,b], N. Redaelli[a], T. Tabarelli de Fatis[a,b], D. Zuolo[a]

JHEP01(2024)101

INFN Sezione di Napoli[a], Università di Napoli 'Federico II'[b], Napoli, Italy; Università della Basilicata[c], Potenza, Italy; Università G. Marconi[d], Roma, Italy

S. Buontempo[a], A. Cagnotta[a,b], F. Carnevali[a,b], N. Cavallo[a,c], A. De Iorio[a,b], F. Fabozzi[a,c], A.O.M. Iorio[a,b], L. Lista[a,b,50], P. Paolucci[a,28], B. Rossi[a], C. Sciacca[a,b]

INFN Sezione di Padova[a], Università di Padova[b], Padova, Italy; Università di Trento[c], Trento, Italy

R. Ardino[a], P. Azzi[a], N. Bacchetta[a,51], D. Bisello[a,b], P. Bortignon[a], A. Bragagnolo[a,b], R. Carlin[a,b], P. Checchia[a], T. Dorigo[a], F. Gasparini[a,b], G. Grosso[a], L. Layer[a,52], E. Lusiani[a], M. Margoni[a,b], A.T. Meneguzzo[a,b], M. Migliorini[a,b], J. Pazzini[a,b], P. Ronchese[a,b], R. Rossin[a,b], M. Sgaravatto[a], F. Simonetto[a,b], G. Strong[a], M. Tosi[a,b], A. Triossi[a,b], S. Ventura[a], H. Yarar[a,b], M. Zanetti[a,b], P. Zotto[a,b], A. Zucchetta[a,b], G. Zumerle[a,b]

INFN Sezione di Pavia[a], Università di Pavia[b], Pavia, Italy

S. Abu Zeid[a,53], C. Aimè[a,b], A. Braghieri[a], S. Calzaferri[a,b], D. Fiorina[a,b], P. Montagna[a,b], V. Re[a], C. Riccardi[a,b], P. Salvini[a], I. Vai[a,b], P. Vitulo[a,b]

INFN Sezione di Perugia[a], Università di Perugia[b], Perugia, Italy

S. Ajmal[a,b], P. Asenov[a,54], G.M. Bilei[a], D. Ciangottini[a,b], L. Fanò[a,b], M. Magherini[a,b], G. Mantovani[a,b], V. Mariani[a,b], M. Menichelli[a], F. Moscatelli[a,54], A. Piccinelli[a,b], M. Presilla[a,b], A. Rossi[a,b], A. Santocchia[a,b], D. Spiga[a], T. Tedeschi[a,b]

INFN Sezione di Pisa[a], Università di Pisa[b], Scuola Normale Superiore di Pisa[c], Pisa, Italy; Università di Siena[d], Siena, Italy

P. Azzurri[a], G. Bagliesi[a], R. Bhattacharya[a], L. Bianchini[a,b], T. Boccali[a], E. Bossini[a], D. Bruschini[a,c], R. Castaldi[a], M.A. Ciocci[a,b], M. Cipriani[a,b], V. D'Amante[a,d], R. Dell'Orso[a], S. Donato[a], A. Giassi[a], F. Ligabue[a,c], D. Matos Figueiredo[a], A. Messineo[a,b], M. Musich[a,b], F. Palla[a], S. Parolia[a], A. Rizzi[a,b], G. Rolandi[a,c], S. Roy Chowdhury[a], T. Sarkar[a], A. Scribano[a], P. Spagnolo[a], R. Tenchini[a,b], G. Tonelli[a,b], N. Turini[a,d], A. Venturi[a], P.G. Verdini[a]

INFN Sezione di Roma[a], Sapienza Università di Roma[b], Roma, Italy

P. Barria[a], M. Campana[a,b], F. Cavallari[a], L. Cunqueiro Mendez[a,b], D. Del Re[a,b], E. Di Marco[a], M. Diemoz[a], F. Errico[a,b], E. Longo[a,b], P. Meridiani[a], J. Mijuskovic[a,b], G. Organtini[a,b], F. Pandolfi[a], R. Paramatti[a,b], C. Quaranta[a,b], S. Rahatlou[a,b], C. Rovelli[a], F. Santanastasio[a,b], L. Soffi[a], R. Tramontano[a,b]

INFN Sezione di Torino[a], Università di Torino[b], Torino, Italy; Università del Piemonte Orientale[c], Novara, Italy

N. Amapane[a,b], R. Arcidiacono[a,c], S. Argiro[a,b], M. Arneodo[a,c], N. Bartosik[a], R. Bellan[a,b], A. Bellora[a,b], C. Biino[a], N. Cartiglia[a], M. Costa[a,b], R. Covarelli[a,b], N. Demaria[a], L. Finco[a], M. Grippo[a,b], B. Kiani[a,b], F. Legger[a], F. Luongo[a,b], C. Mariotti[a], S. Maselli[a], A. Mecca[a,b], E. Migliore[a,b], M. Monteno[a], R. Mulargia[a], M.M. Obertino[a,b], G. Ortona[a], L. Pacher[a,b], N. Pastrone[a], M. Pelliccioni[a], M. Ruspa[a,c],

JHEP01(2024)101

F. Siviero[a,b], V. Sola[a,b], A. Solano[a,b], D. Soldi[a,b], A. Staiano[a], C. Tarricone[a,b], M. Tornago[a,b], D. Trocino[a], G. Umoret[a,b], E. Vlasov[a,b]

INFN Sezione di Trieste[a], Università di Trieste[b], Trieste, Italy
S. Belforte[a], V. Candelise[a,b], M. Casarsa[a], F. Cossutti[a], K. De Leo[a,b], G. Della Ricca[a,b]

Kyungpook National University, Daegu, Korea
S. Dogra, J. Hong, C. Huh, B. Kim, D.H. Kim, J. Kim, H. Lee, S.W. Lee, C.S. Moon, Y.D. Oh, S.I. Pak, M.S. Ryu, S. Sekmen, Y.C. Yang

Chonnam National University, Institute for Universe and Elementary Particles, Kwangju, Korea
G. Bak, P. Gwak, H. Kim, D.H. Moon

Hanyang University, Seoul, Korea
E. Asilar, D. Kim, T.J. Kim, J.A. Merlin, J. Park

Korea University, Seoul, Korea
S. Choi, S. Han, B. Hong, K. Lee, K.S. Lee, J. Park, S.K. Park, J. Yoo

Kyung Hee University, Department of Physics, Seoul, Korea
J. Goh

Sejong University, Seoul, Korea
H. S. Kim, Y. Kim, S. Lee

Seoul National University, Seoul, Korea
J. Almond, J.H. Bhyun, J. Choi, S. Jeon, W. Jun, J. Kim, J.S. Kim, S. Ko, H. Kwon, H. Lee, J. Lee, J. Lee, S. Lee, B.H. Oh, S.B. Oh, H. Seo, U.K. Yang, I. Yoon

University of Seoul, Seoul, Korea
W. Jang, D.Y. Kang, Y. Kang, S. Kim, B. Ko, J.S.H. Lee, Y. Lee, I.C. Park, Y. Roh, I.J. Watson, S. Yang

Yonsei University, Department of Physics, Seoul, Korea
S. Ha, H.D. Yoo

Sungkyunkwan University, Suwon, Korea
M. Choi, M.R. Kim, H. Lee, Y. Lee, I. Yu

College of Engineering and Technology, American University of the Middle East (AUM), Dasman, Kuwait
T. Beyrouthy, Y. Maghrbi

Riga Technical University, Riga, Latvia
K. Dreimanis, A. Gaile, G. Pikurs, A. Potrebko, M. Seidel, V. Veckalns[55]

JHEP01(2024)101

University of Latvia (LU), Riga, Latvia
N.R. Strautnieks

Vilnius University, Vilnius, Lithuania
M. Ambrozas, A. Juodagalvis, A. Rinkevicius, G. Tamulaitis

National Centre for Particle Physics, Universiti Malaya, Kuala Lumpur, Malaysia
N. Bin Norjoharuddeen, I. Yusuff[56], Z. Zolkapli

Universidad de Sonora (UNISON), Hermosillo, Mexico
J.F. Benitez, A. Castaneda Hernandez, H.A. Encinas Acosta, L.G. Gallegos Maríñez, M. León Coello, J.A. Murillo Quijada, A. Sehrawat, L. Valencia Palomo

Centro de Investigacion y de Estudios Avanzados del IPN, Mexico City, Mexico
G. Ayala, H. Castilla-Valdez, E. De La Cruz-Burelo, I. Heredia-De La Cruz[57], R. Lopez-Fernandez, C.A. Mondragon Herrera, A. Sánchez Hernández

Universidad Iberoamericana, Mexico City, Mexico
C. Oropeza Barrera, M. Ramírez García

Benemerita Universidad Autonoma de Puebla, Puebla, Mexico
I. Bautista, I. Pedraza, H.A. Salazar Ibarguen, C. Uribe Estrada

University of Montenegro, Podgorica, Montenegro
I. Bubanja, N. Raicevic

University of Canterbury, Christchurch, New Zealand
P.H. Butler

National Centre for Physics, Quaid-I-Azam University, Islamabad, Pakistan
A. Ahmad, M.I. Asghar, A. Awais, M.I.M. Awan, H.R. Hoorani, W.A. Khan

AGH University of Krakow, Faculty of Computer Science, Electronics and Telecommunications, Krakow, Poland
V. Avati, L. Grzanka, M. Malawski

National Centre for Nuclear Research, Swierk, Poland
H. Bialkowska, M. Bluj, B. Boimska, M. Górski, M. Kazana, M. Szleper, P. Zalewski

Institute of Experimental Physics, Faculty of Physics, University of Warsaw, Warsaw, Poland
K. Bunkowski, K. Doroba, A. Kalinowski, M. Konecki, J. Krolikowski, A. Muhammad

Laboratório de Instrumentação e Física Experimental de Partículas, Lisboa, Portugal
M. Araujo, D. Bastos, C. Beirão Da Cruz E Silva, A. Boletti, M. Bozzo, P. Faccioli, M. Gallinaro, J. Hollar, N. Leonardo, T. Niknejad, A. Petrilli, M. Pisano, J. Seixas, J. Varela

JHEP01(2024)101

Faculty of Physics, University of Belgrade, Belgrade, Serbia
P. Adzic, P. Milenovic

VINCA Institute of Nuclear Sciences, University of Belgrade, Belgrade, Serbia
M. Dordevic, J. Milosevic, V. Rekovic

Centro de Investigaciones Energéticas Medioambientales y Tecnológicas (CIEMAT), Madrid, Spain
M. Aguilar-Benitez, J. Alcaraz Maestre, M. Barrio Luna, Cristina F. Bedoya, M. Cepeda, M. Cerrada, N. Colino, B. De La Cruz, A. Delgado Peris, D. Fernández Del Val, J.P. Fernández Ramos, J. Flix, M.C. Fouz, O. Gonzalez Lopez, S. Goy Lopez, J.M. Hernandez, M.I. Josa, J. León Holgado, D. Moran, C. M. Morcillo Perez, Á. Navarro Tobar, C. Perez Dengra, A. Pérez-Calero Yzquierdo, J. Puerta Pelayo, I. Redondo, D.D. Redondo Ferrero, L. Romero, S. Sánchez Navas, L. Urda Gómez, J. Vazquez Escobar, C. Willmott

Universidad Autónoma de Madrid, Madrid, Spain
J.F. de Trocóniz

Universidad de Oviedo, Instituto Universitario de Ciencias y Tecnologías Espaciales de Asturias (ICTEA), Oviedo, Spain
B. Alvarez Gonzalez, J. Cuevas, J. Fernandez Menendez, S. Folgueras, I. Gonzalez Caballero, J.R. González Fernández, E. Palencia Cortezon, C. Ramón Álvarez, V. Rodríguez Bouza, A. Soto Rodríguez, A. Trapote, C. Vico Villalba, P. Vischia

Instituto de Física de Cantabria (IFCA), CSIC-Universidad de Cantabria, Santander, Spain
S. Bhowmik, S. Blanco Fernández, J.A. Brochero Cifuentes, I.J. Cabrillo, A. Calderon, J. Duarte Campderros, M. Fernandez, C. Fernandez Madrazo, G. Gomez, C. Lasaosa García, C. Martinez Rivero, P. Martinez Ruiz del Arbol, F. Matorras, P. Matorras Cuevas, E. Navarrete Ramos, J. Piedra Gomez, C. Prieels, L. Scodellaro, I. Vila, J.M. Vizan Garcia

University of Colombo, Colombo, Sri Lanka
M.K. Jayananda, B. Kailasapathy[58], D.U.J. Sonnadara, D.D.C. Wickramarathna

University of Ruhuna, Department of Physics, Matara, Sri Lanka
W.G.D. Dharmaratna, K. Liyanage, N. Perera, N. Wickramage

CERN, European Organization for Nuclear Research, Geneva, Switzerland
D. Abbaneo, C. Amendola, E. Auffray, G. Auzinger, J. Baechler, D. Barney, A. Bermúdez Martínez, M. Bianco, B. Bilin, A.A. Bin Anuar, A. Bocci, E. Brondolin, C. Caillol, T. Camporesi, G. Cerminara, N. Chernyavskaya, D. d'Enterria, A. Dabrowski, A. David, A. De Roeck, M.M. Defranchis, M. Deile, M. Dobson, F. Fallavollita[59], L. Forthomme, G. Franzoni, W. Funk, S. Giani, D. Gigi, K. Gill, F. Glege, L. Gouskos, M. Haranko, J. Hegeman, V. Innocente, T. James, P. Janot,

JHEP01(2024)101

J. Kieseler, S. Laurila, P. Lecoq, E. Leutgeb, C. Lourenço, B. Maier, L. Malgeri, M. Mannelli, A.C. Marini, F. Meijers, S. Mersi, E. Meschi, V. Milosevic, F. Moortgat, M. Mulders, S. Orfanelli, F. Pantaleo, M. Peruzzi, G. Petrucciani, A. Pfeiffer, M. Pierini, D. Piparo, H. Qu, D. Rabady, G. Reales Gutiérrez, M. Rovere, H. Sakulin, S. Scarfi, M. Selvaggi, A. Sharma, K. Shchelina, P. Silva, P. Sphicas[60], A.G. Stahl Leiton, A. Steen, S. Summers, D. Treille, P. Tropea, A. Tsirou, D. Walter, J. Wanczyk[61], K.A. Wozniak[62], P. Zehetner, P. Zejdl, W.D. Zeuner

Paul Scherrer Institut, Villigen, Switzerland

T. Bevilacqua[63], L. Caminada[63], A. Ebrahimi, W. Erdmann, R. Horisberger, Q. Ingram, H.C. Kaestli, D. Kotlinski, C. Lange, M. Missiroli[63], L. Noehte[63], T. Rohe

ETH Zurich — Institute for Particle Physics and Astrophysics (IPA), Zurich, Switzerland

T.K. Aarrestad, K. Androsov[61], M. Backhaus, A. Calandri, C. Cazzaniga, K. Datta, A. De Cosa, G. Dissertori, M. Dittmar, M. Donegà, F. Eble, M. Galli, K. Gedia, F. Glessgen, C. Grab, D. Hits, W. Lustermann, A.-M. Lyon, R.A. Manzoni, M. Marchegiani, L. Marchese, C. Martin Perez, A. Mascellani[61], F. Nessi-Tedaldi, F. Pauss, V. Perovic, S. Pigazzini, M.G. Ratti, M. Reichmann, C. Reissel, T. Reitenspiess, B. Ristic, F. Riti, D. Ruini, D.A. Sanz Becerra, R. Seidita, J. Steggemann[61], D. Valsecchi, R. Wallny

Universität Zürich, Zurich, Switzerland

C. Amsler[64], P. Bärtschi, C. Botta, D. Brzhechko, M.F. Canelli, K. Cormier, R. Del Burgo, J.K. Heikkilä, M. Huwiler, W. Jin, A. Jofrehei, B. Kilminster, S. Leontsinis, S.P. Liechti, A. Macchiolo, P. Meiring, V.M. Mikuni, U. Molinatti, I. Neutelings, A. Reimers, P. Robmann, S. Sanchez Cruz, K. Schweiger, M. Senger, Y. Takahashi

National Central University, Chung-Li, Taiwan

C. Adloff[65], C.M. Kuo, W. Lin, P.K. Rout, P.C. Tiwari[39], S.S. Yu

National Taiwan University (NTU), Taipei, Taiwan

L. Ceard, Y. Chao, K.F. Chen, P.s. Chen, Z.g. Chen, W.-S. Hou, T.h. Hsu, Y.w. Kao, R. Khurana, G. Kole, Y.y. Li, R.-S. Lu, E. Paganis, A. Psallidas, X.f. Su, J. Thomas-Wilsker, H.y. Wu, E. Yazgan

High Energy Physics Research Unit, Department of Physics, Faculty of Science, Chulalongkorn University, Bangkok, Thailand

C. Asawatangtrakuldee, N. Srimanobhas, V. Wachirapusitanand

Çukurova University, Physics Department, Science and Art Faculty, Adana, Turkey

D. Agyel, F. Boran, Z.S. Demiroglu, F. Dolek, I. Dumanoglu[66], E. Eskut, Y. Guler[67], E. Gurpinar Guler[67], C. Isik, O. Kara, A. Kayis Topaksu, U. Kiminsu, G. Onengut, K. Ozdemir[68], A. Polatoz, B. Tali[69], U.G. Tok, S. Turkcapar, E. Uslan, I.S. Zorbakir

JHEP01(2024)101

Middle East Technical University, Physics Department, Ankara, Turkey
K. Ocalan[70], M. Yalvac[71]

Bogazici University, Istanbul, Turkey
B. Akgun, I.O. Atakisi, E. Gülmez, M. Kaya[72], O. Kaya[73], S. Tekten[74]

Istanbul Technical University, Istanbul, Turkey
A. Cakir, K. Cankocak[66], Y. Komurcu, S. Sen[75]

Istanbul University, Istanbul, Turkey
O. Aydilek, S. Cerci[69], V. Epshteyn, B. Hacisahinoglu, I. Hos[76], B. Isildak[77], B. Kaynak, S. Ozkorucuklu, O. Potok, H. Sert, C. Simsek, D. Sunar Cerci[69], C. Zorbilmez

Institute for Scintillation Materials of National Academy of Science of Ukraine, Kharkiv, Ukraine
A. Boyaryntsev, B. Grynyov

National Science Centre, Kharkiv Institute of Physics and Technology, Kharkiv, Ukraine
L. Levchuk

University of Bristol, Bristol, United Kingdom
D. Anthony, J.J. Brooke, A. Bundock, F. Bury, E. Clement, D. Cussans, H. Flacher, M. Glowacki, J. Goldstein, H.F. Heath, L. Kreczko, B. Krikler, S. Paramesvaran, S. Seif El Nasr-Storey, V.J. Smith, N. Stylianou[78], K. Walkingshaw Pass, R. White

Rutherford Appleton Laboratory, Didcot, United Kingdom
A.H. Ball, K.W. Bell, A. Belyaev[79], C. Brew, R.M. Brown, D.J.A. Cockerill, C. Cooke, K.V. Ellis, K. Harder, S. Harper, M.-L. Holmberg[80], Sh. Jain, J. Linacre, K. Manolopoulos, D.M. Newbold, E. Olaiya, D. Petyt, T. Reis, G. Salvi, T. Schuh, C.H. Shepherd-Themistocleous, I.R. Tomalin, T. Williams

Imperial College, London, United Kingdom
R. Bainbridge, P. Bloch, C.E. Brown, O. Buchmuller, V. Cacchio, C.A. Carrillo Montoya, G.S. Chahal[81], D. Colling, J.S. Dancu, P. Dauncey, G. Davies, J. Davies, M. Della Negra, S. Fayer, G. Fedi, G. Hall, M.H. Hassanshahi, A. Howard, G. Iles, M. Knight, J. Langford, L. Lyons, A.-M. Magnan, S. Malik, A. Martelli, M. Mieskolainen, J. Nash[82], M. Pesaresi, B.C. Radburn-Smith, A. Richards, A. Rose, C. Seez, R. Shukla, A. Tapper, K. Uchida, G.P. Uttley, L.H. Vage, T. Virdee[28], M. Vojinovic, N. Wardle, D. Winterbottom

Brunel University, Uxbridge, United Kingdom
K. Coldham, J.E. Cole, A. Khan, P. Kyberd, I.D. Reid

JHEP01(2024)101

Baylor University, Waco, Texas, U.S.A.

S. Abdullin, A. Brinkerhoff, B. Caraway, J. Dittmann, K. Hatakeyama, J. Hiltbrand, A.R. Kanuganti, B. McMaster, M. Saunders, S. Sawant, C. Sutantawibul, M. Toms[83], J. Wilson

Catholic University of America, Washington, DC, U.S.A.

R. Bartek, A. Dominguez, C. Huerta Escamilla, A.E. Simsek, R. Uniyal, A.M. Vargas Hernandez

The University of Alabama, Tuscaloosa, Alabama, U.S.A.

R. Chudasama, S.I. Cooper, S.V. Gleyzer, C.U. Perez, P. Rumerio[84], E. Usai, C. West, R. Yi

Boston University, Boston, Massachusetts, U.S.A.

A. Akpinar, A. Albert, D. Arcaro, C. Cosby, Z. Demiragli, C. Erice, E. Fontanesi, D. Gastler, J. Rohlf, K. Salyer, D. Sperka, D. Spitzbart, I. Suarez, A. Tsatsos, S. Yuan

Brown University, Providence, Rhode Island, U.S.A.

G. Benelli, X. Coubez[23], D. Cutts, M. Hadley, U. Heintz, J.M. Hogan[85], T. Kwon, G. Landsberg, K.T. Lau, D. Li, J. Luo, S. Mondal, M. Narain[†], N. Pervan, S. Sagir[86], F. Simpson, M. Stamenkovic, W.Y. Wong, X. Yan, W. Zhang

University of California, Davis, Davis, California, U.S.A.

S. Abbott, J. Bonilla, C. Brainerd, R. Breedon, M. Calderon De La Barca Sanchez, M. Chertok, M. Citron, J. Conway, P.T. Cox, R. Erbacher, G. Haza, F. Jensen, O. Kukral, G. Mocellin, M. Mulhearn, D. Pellett, B. Regnery, W. Wei, Y. Yao, F. Zhang

University of California, Los Angeles, California, U.S.A.

M. Bachtis, R. Cousins, A. Datta, J. Hauser, M. Ignatenko, M.A. Iqbal, T. Lam, E. Manca, W.A. Nash, D. Saltzberg, B. Stone, V. Valuev

University of California, Riverside, Riverside, California, U.S.A.

R. Clare, M. Gordon, G. Hanson, W. Si, S. Wimpenny[†]

University of California, San Diego, La Jolla, California, U.S.A.

J.G. Branson, S. Cittolin, S. Cooperstein, D. Diaz, J. Duarte, R. Gerosa, L. Giannini, J. Guiang, R. Kansal, V. Krutelyov, R. Lee, J. Letts, M. Masciovecchio, F. Mokhtar, M. Pieri, M. Quinnan, B.V. Sathia Narayanan, V. Sharma, M. Tadel, E. Vourliotis, F. Würthwein, Y. Xiang, A. Yagil

University of California, Santa Barbara — Department of Physics, Santa Barbara, California, U.S.A.

A. Barzdukas, L. Brennan, C. Campagnari, G. Collura, A. Dorsett, J. Incandela, M. Kilpatrick, J. Kim, A.J. Li, P. Masterson, H. Mei, M. Oshiro, J. Richman, U. Sarica, R. Schmitz, F. Setti, J. Sheplock, D. Stuart, S. Wang

JHEP01(2024)101

California Institute of Technology, Pasadena, California, U.S.A.
A. Bornheim, O. Cerri, A. Latorre, J.M. Lawhorn, J. Mao, H.B. Newman, T. Q. Nguyen, M. Spiropulu, J.R. Vlimant, C. Wang, S. Xie, R.Y. Zhu

Carnegie Mellon University, Pittsburgh, Pennsylvania, U.S.A.
J. Alison, S. An, M.B. Andrews, P. Bryant, V. Dutta, T. Ferguson, A. Harilal, C. Liu, T. Mudholkar, S. Murthy, M. Paulini, A. Roberts, A. Sanchez, W. Terrill

University of Colorado Boulder, Boulder, Colorado, U.S.A.
J.P. Cumalat, W.T. Ford, A. Hassani, G. Karathanasis, E. MacDonald, N. Manganelli, F. Marini, A. Perloff, C. Savard, N. Schonbeck, K. Stenson, K.A. Ulmer, S.R. Wagner, N. Zipper

Cornell University, Ithaca, New York, U.S.A.
J. Alexander, S. Bright-Thonney, X. Chen, D.J. Cranshaw, J. Fan, X. Fan, D. Gadkari, S. Hogan, J. Monroy, J.R. Patterson, J. Reichert, M. Reid, A. Ryd, J. Thom, P. Wittich, R. Zou

Fermi National Accelerator Laboratory, Batavia, Illinois, U.S.A.
M. Albrow, M. Alyari, O. Amram, G. Apollinari, A. Apresyan, L.A.T. Bauerdick, D. Berry, J. Berryhill, P.C. Bhat, K. Burkett, J.N. Butler, A. Canepa, G.B. Cerati, H.W.K. Cheung, F. Chlebana, G. Cummings, J. Dickinson, I. Dutta, V.D. Elvira, Y. Feng, J. Freeman, A. Gandrakota, Z. Gecse, L. Gray, D. Green, S. Grünendahl, D. Guerrero, O. Gutsche, R.M. Harris, R. Heller, T.C. Herwig, J. Hirschauer, L. Horyn, B. Jayatilaka, S. Jindariani, M. Johnson, U. Joshi, T. Klijnsma, B. Klima, K.H.M. Kwok, S. Lammel, D. Lincoln, R. Lipton, T. Liu, C. Madrid, K. Maeshima, C. Mantilla, D. Mason, P. McBride, P. Merkel, S. Mrenna, S. Nahn, J. Ngadiuba, D. Noonan, V. Papadimitriou, N. Pastika, K. Pedro, C. Pena[87], F. Ravera, A. Reinsvold Hall[88], L. Ristori, E. Sexton-Kennedy, N. Smith, A. Soha, L. Spiegel, S. Stoynev, J. Strait, L. Taylor, S. Tkaczyk, N.V. Tran, L. Uplegger, E.W. Vaandering, I. Zoi

University of Florida, Gainesville, Florida, U.S.A.
C. Aruta, P. Avery, D. Bourilkov, L. Cadamuro, P. Chang, V. Cherepanov, R.D. Field, E. Koenig, M. Kolosova, J. Konigsberg, A. Korytov, K.H. Lo, K. Matchev, N. Menendez, G. Mitselmakher, A. Muthirakalayil Madhu, N. Rawal, D. Rosenzweig, S. Rosenzweig, K. Shi, J. Wang

Florida State University, Tallahassee, Florida, U.S.A.
T. Adams, A. Al Kadhim, A. Askew, N. Bower, R. Habibullah, V. Hagopian, R. Hashmi, R.S. Kim, S. Kim, T. Kolberg, G. Martinez, H. Prosper, P.R. Prova, O. Viazlo, M. Wulansatiti, R. Yohay, J. Zhang

Florida Institute of Technology, Melbourne, Florida, U.S.A.
B. Alsufyani, M.M. Baarmand, S. Butalla, T. Elkafrawy[53], M. Hohlmann, R. Kumar Verma, M. Rahmani

JHEP01(2024)101

University of Illinois Chicago, Chicago, U.S.A., Chicago, U.S.A.

M.R. Adams, C. Bennett, R. Cavanaugh, S. Dittmer, R. Escobar Franco, O. Evdokimov, C.E. Gerber, D.J. Hofman, J.h. Lee, D. S. Lemos, A.H. Merrit, C. Mills, S. Nanda, G. Oh, B. Ozek, D. Pilipovic, T. Roy, S. Rudrabhatla, M.B. Tonjes, N. Varelas, X. Wang, Z. Ye, J. Yoo

The University of Iowa, Iowa City, Iowa, U.S.A.

M. Alhusseini, D. Blend, K. Dilsiz[89], L. Emediato, G. Karaman, O.K. Köseyan, J.-P. Merlo, A. Mestvirishvili[90], J. Nachtman, O. Neogi, H. Ogul[91], Y. Onel, A. Penzo, C. Snyder, E. Tiras[92]

Johns Hopkins University, Baltimore, Maryland, U.S.A.

B. Blumenfeld, L. Corcodilos, J. Davis, A.V. Gritsan, L. Kang, S. Kyriacou, P. Maksimovic, M. Roguljic, J. Roskes, S. Sekhar, M. Swartz, T.Á. Vámi

The University of Kansas, Lawrence, Kansas, U.S.A.

A. Abreu, L.F. Alcerro Alcerro, J. Anguiano, P. Baringer, A. Bean, Z. Flowers, D. Grove, J. King, G. Krintiras, M. Lazarovits, C. Le Mahieu, C. Lindsey, J. Marquez, N. Minafra, M. Murray, M. Nickel, M. Pitt, S. Popescu[93], C. Rogan, C. Royon, R. Salvatico, S. Sanders, C. Smith, Q. Wang, G. Wilson

Kansas State University, Manhattan, Kansas, U.S.A.

B. Allmond, A. Ivanov, K. Kaadze, A. Kalogeropoulos, D. Kim, Y. Maravin, K. Nam, J. Natoli, D. Roy, G. Sorrentino

Lawrence Livermore National Laboratory, Livermore, California, U.S.A.

F. Rebassoo, D. Wright

University of Maryland, College Park, Maryland, U.S.A.

E. Adams, A. Baden, O. Baron, A. Belloni, A. Bethani, Y.M. Chen, S.C. Eno, N.J. Hadley, S. Jabeen, R.G. Kellogg, T. Koeth, Y. Lai, S. Lascio, A.C. Mignerey, S. Nabili, C. Palmer, C. Papageorgakis, M.M. Paranjpe, L. Wang, K. Wong

Massachusetts Institute of Technology, Cambridge, Massachusetts, U.S.A.

J. Bendavid, W. Busza, I.A. Cali, Y. Chen, M. D'Alfonso, J. Eysermans, C. Freer, G. Gomez-Ceballos, M. Goncharov, P. Harris, D. Hoang, D. Kovalskyi, J. Krupa, L. Lavezzo, Y.-J. Lee, K. Long, C. Mironov, C. Paus, D. Rankin, C. Roland, G. Roland, S. Rothman, Z. Shi, G.S.F. Stephans, J. Wang, Z. Wang, B. Wyslouch, T. J. Yang

University of Minnesota, Minneapolis, Minnesota, U.S.A.

B. Crossman, B.M. Joshi, C. Kapsiak, M. Krohn, D. Mahon, J. Mans, B. Marzocchi, S. Pandey, M. Revering, R. Rusack, R. Saradhy, N. Schroeder, N. Strobbe, M.A. Wadud

University of Mississippi, Oxford, Mississippi, U.S.A.

L.M. Cremaldi

JHEP01(2024)101

University of Nebraska-Lincoln, Lincoln, Nebraska, U.S.A.
K. Bloom, M. Bryson, D.R. Claes, C. Fangmeier, F. Golf, J. Hossain, C. Joo, I. Kravchenko, I. Reed, J.E. Siado, G.R. Snow†, W. Tabb, A. Vagnerini, A. Wightman, F. Yan, D. Yu, A.G. Zecchinelli

State University of New York at Buffalo, Buffalo, New York, U.S.A.
G. Agarwal, H. Bandyopadhyay, L. Hay, I. Iashvili, A. Kharchilava, C. McLean, M. Morris, D. Nguyen, J. Pekkanen, S. Rappoccio, H. Rejeb Sfar, A. Williams

Northeastern University, Boston, Massachusetts, U.S.A.
G. Alverson, E. Barberis, Y. Haddad, Y. Han, A. Krishna, J. Li, M. Lu, G. Madigan, D.M. Morse, V. Nguyen, T. Orimoto, A. Parker, L. Skinnari, A. Tishelman-Charny, B. Wang, D. Wood

Northwestern University, Evanston, Illinois, U.S.A.
S. Bhattacharya, J. Bueghly, Z. Chen, K.A. Hahn, Y. Liu, Y. Miao, D.G. Monk, M.H. Schmitt, A. Taliercio, M. Velasco

University of Notre Dame, Notre Dame, Indiana, U.S.A.
R. Band, R. Bucci, S. Castells, M. Cremonesi, A. Das, R. Goldouzian, M. Hildreth, K.W. Ho, K. Hurtado Anampa, C. Jessop, K. Lannon, J. Lawrence, N. Loukas, L. Lutton, J. Mariano, N. Marinelli, I. Mcalister, T. McCauley, C. Mcgrady, K. Mohrman, C. Moore, Y. Musienko[13], H. Nelson, M. Osherson, R. Ruchti, A. Townsend, M. Wayne, H. Yockey, M. Zarucki, L. Zygala

The Ohio State University, Columbus, Ohio, U.S.A.
A. Basnet, B. Bylsma, M. Carrigan, L.S. Durkin, C. Hill, M. Joyce, A. Lesauvage, M. Nunez Ornelas, K. Wei, B.L. Winer, B. R. Yates

Princeton University, Princeton, New Jersey, U.S.A.
F.M. Addesa, H. Bouchamaoui, P. Das, G. Dezoort, P. Elmer, A. Frankenthal, B. Greenberg, N. Haubrich, S. Higginbotham, G. Kopp, S. Kwan, D. Lange, A. Loeliger, D. Marlow, I. Ojalvo, J. Olsen, D. Stickland, C. Tully

University of Puerto Rico, Mayaguez, Puerto Rico, U.S.A.
S. Malik

Purdue University, West Lafayette, Indiana, U.S.A.
A.S. Bakshi, V.E. Barnes, S. Chandra, R. Chawla, S. Das, A. Gu, L. Gutay, M. Jones, A.W. Jung, D. Kondratyev, A.M. Koshy, M. Liu, G. Negro, N. Neumeister, G. Paspalaki, S. Piperov, A. Purohit, J.F. Schulte, M. Stojanovic, J. Thieman, A. K. Virdi, F. Wang, W. Xie

Purdue University Northwest, Hammond, Indiana, U.S.A.
J. Dolen, N. Parashar, A. Pathak

JHEP01(2024)101

Rice University, Houston, Texas, U.S.A.

D. Acosta, A. Baty, T. Carnahan, S. Dildick, K.M. Ecklund, P.J. Fernández Manteca, S. Freed, P. Gardner, F.J.M. Geurts, A. Kumar, W. Li, O. Miguel Colin, B.P. Padley, R. Redjimi, J. Rotter, E. Yigitbasi, Y. Zhang

University of Rochester, Rochester, New York, U.S.A.

A. Bodek, P. de Barbaro, R. Demina, J.L. Dulemba, C. Fallon, A. Garcia-Bellido, O. Hindrichs, A. Khukhunaishvili, P. Parygin[83], E. Popova[83], R. Taus, G.P. Van Onsem

The Rockefeller University, New York, New York, U.S.A.

K. Goulianos

Rutgers, The State University of New Jersey, Piscataway, New Jersey, U.S.A.

B. Chiarito, J.P. Chou, Y. Gershtein, E. Halkiadakis, A. Hart, M. Heindl, D. Jaroslawski, O. Karacheban[26], I. Laflotte, A. Lath, R. Montalvo, K. Nash, H. Routray, S. Salur, S. Schnetzer, S. Somalwar, R. Stone, S.A. Thayil, S. Thomas, J. Vora, H. Wang

University of Tennessee, Knoxville, Tennessee, U.S.A.

H. Acharya, D. Ally, A.G. Delannoy, S. Fiorendi, T. Holmes, N. Karunarathna, L. Lee, E. Nibigira, S. Spanier

Texas A&M University, College Station, Texas, U.S.A.

D. Aebi, M. Ahmad, O. Bouhali[94], M. Dalchenko, R. Eusebi, J. Gilmore, T. Huang, T. Kamon[95], H. Kim, S. Luo, S. Malhotra, R. Mueller, D. Overton, D. Rathjens, A. Safonov

Texas Tech University, Lubbock, Texas, U.S.A.

N. Akchurin, J. Damgov, V. Hegde, A. Hussain, Y. Kazhykarim, K. Lamichhane, S.W. Lee, A. Mankel, T. Mengke, S. Muthumuni, T. Peltola, I. Volobouev, A. Whitbeck

Vanderbilt University, Nashville, Tennessee, U.S.A.

E. Appelt, S. Greene, A. Gurrola, W. Johns, R. Kunnawalkam Elayavalli, A. Melo, F. Romeo, P. Sheldon, S. Tuo, J. Velkovska, J. Viinikainen

University of Virginia, Charlottesville, Virginia, U.S.A.

B. Cardwell, B. Cox, J. Hakala, R. Hirosky, A. Ledovskoy, A. Li, C. Neu, C.E. Perez Lara

Wayne State University, Detroit, Michigan, U.S.A.

P.E. Karchin

University of Wisconsin — Madison, Madison, Wisconsin, U.S.A.

A. Aravind, S. Banerjee, K. Black, T. Bose, S. Dasu, I. De Bruyn, P. Everaerts, C. Galloni, H. He, M. Herndon, A. Herve, C.K. Koraka, A. Lanaro, R. Loveless, J. Madhusudanan Sreekala, A. Mallampalli, A. Mohammadi, S. Mondal, G. Parida,

JHEP01(2024)101

D. Pinna, A. Savin, V. Shang, V. Sharma, W.H. Smith, D. Teague, H.F. Tsoi, W. Vetens, A. Warden

Authors affiliated with an institute or an international laboratory covered by a cooperation agreement with CERN

S. Afanasiev, V. Andreev, Yu. Andreev, T. Aushev, M. Azarkin, A. Babaev, A. Belyaev, V. Blinov[96], E. Boos, V. Borshch, D. Budkouski, V. Bunichev, M. Chadeeva[96], V. Chekhovsky, M. Danilov[96], A. Dermenev, T. Dimova[96], D. Druzhkin[97], M. Dubinin[87], L. Dudko, G. Gavrilov, V. Gavrilov, S. Gninenko, V. Golovtcov, N. Golubev, I. Golutvin, I. Gorbunov, Y. Ivanov, V. Kachanov, L. Kardapoltsev[96], V. Karjavine, A. Karneyeu, V. Kim[96], M. Kirakosyan, D. Kirpichnikov, M. Kirsanov, V. Klyukhin, O. Kodolova[98], D. Konstantinov, V. Korenkov, A. Kozyrev[96], N. Krasnikov, A. Lanev, P. Levchenko[99], O. Lukina, N. Lychkovskaya, V. Makarenko, A. Malakhov, V. Matveev[96], V. Murzin, A. Nikitenko[100,98], S. Obraztsov, V. Oreshkin, A. Oskin, V. Palichik, V. Perelygin, S. Petrushanko, V. Popov, O. Radchenko[96], V. Rusinov, M. Savina, V. Savrin, V. Shalaev, S. Shmatov, S. Shulha, Y. Skovpen[96], S. Slabospitskii, V. Smirnov, A. Snigirev, D. Sosnov, V. Sulimov, E. Tcherniaev, A. Terkulov, O. Teryaev, I. Tlisova, A. Toropin, L. Uvarov, A. Uzunian, A. Vorobyev[†], N. Voytishin, B.S. Yuldashev[101], A. Zarubin, I. Zhizhin, A. Zhokin

[†] *Deceased*
[1] *Also at Yerevan State University, Yerevan, Armenia*
[2] *Also at TU Wien, Vienna, Austria*
[3] *Also at Institute of Basic and Applied Sciences, Faculty of Engineering, Arab Academy for Science, Technology and Maritime Transport, Alexandria, Egypt*
[4] *Also at Ghent University, Ghent, Belgium*
[5] *Also at Universidade Estadual de Campinas, Campinas, Brazil*
[6] *Also at Federal University of Rio Grande do Sul, Porto Alegre, Brazil*
[7] *Also at UFMS, Nova Andradina, Brazil*
[8] *Also at Nanjing Normal University, Nanjing, China*
[9] *Now at The University of Iowa, Iowa City, Iowa, U.S.A.*
[10] *Also at University of Chinese Academy of Sciences, Beijing, China*
[11] *Also at University of Chinese Academy of Sciences, Beijing, China*
[12] *Also at Université Libre de Bruxelles, Bruxelles, Belgium*
[13] *Also at an institute or an international laboratory covered by a cooperation agreement with CERN*
[14] *Also at Suez University, Suez, Egypt*
[15] *Now at British University in Egypt, Cairo, Egypt*
[16] *Also at Birla Institute of Technology, Mesra, Mesra, India*
[17] *Also at Purdue University, West Lafayette, Indiana, U.S.A.*
[18] *Also at Université de Haute Alsace, Mulhouse, France*
[19] *Also at Department of Physics, Tsinghua University, Beijing, China*
[20] *Also at The University of the State of Amazonas, Manaus, Brazil*
[21] *Also at Erzincan Binali Yildirim University, Erzincan, Turkey*
[22] *Also at University of Hamburg, Hamburg, Germany*
[23] *Also at RWTH Aachen University, III. Physikalisches Institut A, Aachen, Germany*
[24] *Also at Isfahan University of Technology, Isfahan, Iran*
[25] *Also at Bergische University Wuppertal (BUW), Wuppertal, Germany*
[26] *Also at Brandenburg University of Technology, Cottbus, Germany*
[27] *Also at Forschungszentrum Jülich, Juelich, Germany*
[28] *Also at CERN, European Organization for Nuclear Research, Geneva, Switzerland*

[29] Also at Physics Department, Faculty of Science, Assiut University, Assiut, Egypt
[30] Also at Wigner Research Centre for Physics, Budapest, Hungary
[31] Also at Institute of Physics, University of Debrecen, Debrecen, Hungary
[32] Also at Institute of Nuclear Research ATOMKI, Debrecen, Hungary
[33] Now at Universitatea Babes-Bolyai — Facultatea de Fizica, Cluj-Napoca, Romania
[34] Also at Faculty of Informatics, University of Debrecen, Debrecen, Hungary
[35] Also at Punjab Agricultural University, Ludhiana, India
[36] Also at UPES — University of Petroleum and Energy Studies, Dehradun, India
[37] Also at University of Visva-Bharati, Santiniketan, India
[38] Also at University of Hyderabad, Hyderabad, India
[39] Also at Indian Institute of Science (IISc), Bangalore, India
[40] Also at IIT Bhubaneswar, Bhubaneswar, India
[41] Also at Institute of Physics, Bhubaneswar, India
[42] Also at Deutsches Elektronen-Synchrotron, Hamburg, Germany
[43] Also at Department of Physics, Isfahan University of Technology, Isfahan, Iran
[44] Also at Sharif University of Technology, Tehran, Iran
[45] Also at Department of Physics, University of Science and Technology of Mazandaran, Behshahr, Iran
[46] Also at Helwan University, Cairo, Egypt
[47] Also at Italian National Agency for New Technologies, Energy and Sustainable Economic Development, Bologna, Italy
[48] Also at Centro Siciliano di Fisica Nucleare e di Struttura Della Materia, Catania, Italy
[49] Also at Università degli Studi Guglielmo Marconi, Roma, Italy
[50] Also at Scuola Superiore Meridionale, Università di Napoli 'Federico II', Napoli, Italy
[51] Also at Fermi National Accelerator Laboratory, Batavia, Illinois, U.S.A.
[52] Also at Università di Napoli 'Federico II', Napoli, Italy
[53] Also at Ain Shams University, Cairo, Egypt
[54] Also at Consiglio Nazionale delle Ricerche — Istituto Officina dei Materiali, Perugia, Italy
[55] Also at Riga Technical University, Riga, Latvia
[56] Also at Department of Applied Physics, Faculty of Science and Technology, Universiti Kebangsaan Malaysia, Bangi, Malaysia
[57] Also at Consejo Nacional de Ciencia y Tecnología, Mexico City, Mexico
[58] Also at Trincomalee Campus, Eastern University, Sri Lanka, Nilaveli, Sri Lanka
[59] Also at INFN Sezione di Pavia, Università di Pavia, Pavia, Italy
[60] Also at National and Kapodistrian University of Athens, Athens, Greece
[61] Also at Ecole Polytechnique Fédérale Lausanne, Lausanne, Switzerland
[62] Also at University of Vienna Faculty of Computer Science, Vienna, Austria
[63] Also at Universität Zürich, Zurich, Switzerland
[64] Also at Stefan Meyer Institute for Subatomic Physics, Vienna, Austria
[65] Also at Laboratoire d'Annecy-le-Vieux de Physique des Particules, IN2P3-CNRS, Annecy-le-Vieux, France
[66] Also at Near East University, Research Center of Experimental Health Science, Mersin, Turkey
[67] Also at Konya Technical University, Konya, Turkey
[68] Also at Izmir Bakircay University, Izmir, Turkey
[69] Also at Adiyaman University, Adiyaman, Turkey
[70] Also at Necmettin Erbakan University, Konya, Turkey
[71] Also at Bozok Universitetesi Rektörlügü, Yozgat, Turkey
[72] Also at Marmara University, Istanbul, Turkey
[73] Also at Milli Savunma University, Istanbul, Turkey
[74] Also at Kafkas University, Kars, Turkey
[75] Also at Hacettepe University, Ankara, Turkey
[76] Also at Istanbul University — Cerrahpasa, Faculty of Engineering, Istanbul, Turkey
[77] Also at Yildiz Technical University, Istanbul, Turkey
[78] Also at Vrije Universiteit Brussel, Brussel, Belgium
[79] Also at School of Physics and Astronomy, University of Southampton, Southampton, United Kingdom

JHEP01(2024)101

[80] *Also at University of Bristol, Bristol, United Kingdom*
[81] *Also at IPPP Durham University, Durham, United Kingdom*
[82] *Also at Monash University, Faculty of Science, Clayton, Australia*
[83] *Now at an institute or an international laboratory covered by a cooperation agreement with CERN*
[84] *Also at Università di Torino, Torino, Italy*
[85] *Also at Bethel University, St. Paul, Minnesota, U.S.A.*
[86] *Also at Karamanoğlu Mehmetbey University, Karaman, Turkey*
[87] *Also at California Institute of Technology, Pasadena, California, U.S.A.*
[88] *Also at United States Naval Academy, Annapolis, Maryland, U.S.A.*
[89] *Also at Bingol University, Bingol, Turkey*
[90] *Also at Georgian Technical University, Tbilisi, Georgia*
[91] *Also at Sinop University, Sinop, Turkey*
[92] *Also at Erciyes University, Kayseri, Turkey*
[93] *Also at Horia Hulubei National Institute of Physics and Nuclear Engineering (IFIN-HH), Bucharest, Romania*
[94] *Also at Texas A&M University at Qatar, Doha, Qatar*
[95] *Also at Kyungpook National University, Daegu, Korea*
[96] *Also at another institute or international laboratory covered by a cooperation agreement with CERN*
[97] *Also at Universiteit Antwerpen, Antwerpen, Belgium*
[98] *Also at Yerevan Physics Institute, Yerevan, Armenia*
[99] *Also at Northeastern University, Boston, Massachusetts, U.S.A.*
[100] *Also at Imperial College, London, United Kingdom*
[101] *Also at Institute of Nuclear Physics of the Uzbekistan Academy of Sciences, Tashkent, Uzbekistan*

JHEP01(2024)101